# Retrosplenial cortex encodes both local and global space in connected environments

**Célia Laurent[1], David Smith[2], Francesca Sargolini[1], Pierre-Yves Jacob[1]**

[1] Aix Marseille Univ, CNRS, CRPN, Marseille, France

[2] Department of Psychology, Cornell University, Ithaca, New York, USA

**Corresponding author:** pierre-yves.jacob@univ-amu.fr

## Abstract

In everyday life, mammals have to find their way between interconnected spaces. How the brain processes spatial information in these complex environments is a crucial question for understanding how we navigate. Theoretical frameworks have proposed that the brain produces simultaneous activities that are either maintained in connected spaces (global reference frame) or distinguished in each space (local reference frames). The different head direction signals discovered in the retrosplenial cortex (RSC) suggest that this brain area supports both local and global spatial activity. We tested this hypothesis by recording RSC neurons in environments consisting of 2 or 4 connected rooms that are either identical or different. We observed two types of head direction activity simultaneously: one showing opposite or orthogonal directional activity in the 2 and 4 connected spaces and thus anchored to local reference frames, and one maintaining a stable head direction activity across connected spaces and thus anchored to the global reference frame. We also found that other RSC neurons show a spatial pattern that repeats oppositely or orthogonally in the 2 and 4 connected spaces respectively. In contrast, hippocampal place cells activity never shows opposite or orthogonal patterns, but rather a spatial remapping or a translational repeated activity. Overall, the results show that only the

RSC has the simultaneous neuronal activity supporting local and global reference frames, necessary to form a spatial representation in connected environments.

# Introduction

Deciphering the spatial systems of the brain in complex spaces is crucial to understand how mammals navigate in ecological conditions. Recent studies have described new classes of spatial-coding neurons in the retrosplenial cortex (RSC), including the multidirectional cells (MDCs) that can be observed only in complex environments made of connected rooms (*Alexander et al., 2020; Jacob et al., 2017; Subramanian & Smith, 2024; Zhang et al., 2022*). In contrast to a head direction cell (HDC) that maintains a unique preferred firing direction (PFD) across different connected rooms, a MDC changes its PFD between rooms leading to a bidirectional or tetradirectional activity in the global polar activity. The discovery of MDCs shows that a single and homogeneous environment such as an open field is not sufficient to reveal the multifaceted activity of the space-coding neurons, and this constitutes a serious limitation in the current models of neural space codes.

The functional role of the MDCs in the RSC is unknown. From a wide perspective, the RSC is involved in a range of cognitive functions, including navigation and episodic memory (*Miller et al. 2019; Mitchell et al., 2018; Sherril et al., 2013; Takahashi et al., 1997; Vann et al., 2009; Vedder et al., 2016*). This is not surprising given the intense anatomical connections between the RSC, the medial entorhinal cortex and the hippocampus which are key structures in spatial cognition (*Burwell & Amaral, 1998; Cenquizca & Swanson, 2007; Czajkowski et al., 2013; Insausti et al., 1997; Jones & Witter, 2007; Naber et al., 2001; Shibata, 1994; Sugar & Witter, 2016; Van Groen & Wyss, 1992, 2003; Vogt & Miller, 1983*).

In addition, the RSC receives strong projections from primary visual areas, and vision has a major role in navigation (*Muller, Kubie & Ranck, 1987; Vélez-Fort et al., 2018; Vogt & Miller, 1983; Wyss & Van Groen, 1992, 2003; Yoder et al., 2011*). Therefore, it is possible that the RSC participates in these functions by processing visual features of the space to anchor the brain directional system to different reference frames. Results from fMRI studies in humans are consistent with this hypothesis but are contradictory as to whether the RSC has a specific role in anchoring the spatial representation to the local or the global reference frame (*Kim & Maguire, 2018; Marchette et al., 2014; Peer et al., 2019; Shine et al., 2016; Sulpizio et al., 2013*). The existence of both HDCs and MDCs within the RSC possibly reconciles these two opposing views. A local reference frame involves a single room limited by walls. For an environment made of several connected rooms, there will be as many local reference frames as there will be rooms visited by the subject. The global reference frame unifies the set of local rooms into a single representation. Since MDCs change their directional firing in connected rooms, they are good candidates for establishing a local reference frame. Conversely, the HDCs may help construct a global reference frame since their directional firing remains stable across different connected rooms.

Studies on MDCs used connected rooms that are visually and tactilely identical, thus making these external features ambiguous to dissociate the rooms. Moreover, the opposite or orthogonal repetition of similar connected rooms could possibly induce an artificial multidirectional firing. To specifically assess whether MDCs firing properties result from a dissociation between the different rooms, we recorded RSC neurons in environments made of 2- or 4-connected-rooms that are different visually and tactilely. We observed that the bidirectional activity in the 2-connected-rooms environment becomes tetradirectional in the 4-connected-rooms environment. In contrast, HDCs remain unidirectional in all environments.

We also observed that neurons with no clear place-related activity (no directional activities and no place fields) nonetheless showed repeated opposite or orthogonal spatial patterns in the 2- and 4-connected-rooms environments, respectively. Finally, we recorded in the same environment the hippocampal place cells and showed that they either remapped or repeated their firing fields between rooms, suggesting that they can be differentially anchored to local or global cues.

Altogether, these results highlight the RSC as a key structure in forming spatial representations at different spatial reference frames, a cognitive process that may be critical for navigating in complex spaces.

# Methods

**Subjects.** A total of 15 adult Long Evans rats (Charles River Laboratories), 12 males and 3 females weighing between 250 and 350g were housed in individual cages (40 cm long x 26 cm wide x 16 cm high) with *ad lib* food and water and kept in a temperature-controlled room (20°C +/- 2°C) with natural light/dark cycle. One week after arrival, animals were handled daily by the experimenter for 7 days. During this period, they were habituated to the recording apparatus by letting them explore the environment for 10–20 min per day.

All experimental procedures were conducted with the approval of the local French National Ethics Committees and in accordance with the EEC (2010/63/UE) guidelines for the care and use of laboratory animals. The present study was specifically approved by Neurosciences Ethics Committee N°71 of the French National Committee of animal experimentation.

**Microdrives and surgery**. Recordings were made using tetrodes, each composed of four twisted 25 µm polyimide-coated platinum-iridium (90%/10%) wires (California Fine Wire, CA), attached to an Axona microdrive (Axona Ltd, St Albans, UK). Surgery was performed under sterile conditions and general anesthesia (Isoflurane, 4% for induction, 2% to 0.5% for maintenance), an opioid analgesic (Buprenorphine, 0.05 mg/kg, SC) is administered at least 30 minutes before. Tetrodes were then stereotaxically implanted in the dysgranular RSC (n = 14 rats; coordinates in mm from Bregma: AP: -5.0 to -5.5mm, ML: +/-0.75 to 1.0mm and DV: 0.4 to 0.5mm under the dura) and/or the dorsal hippocampus (n = 4 rats; coordinates in mm from Bregma: AP: -3.8, ML: +/-3 and DV: 1.5mm under the dura) either in the left or right hemisphere. As a postoperative treatment, rats received an injection of antibiotic (Oxytetracycline, 10 mg/kg) and of anti-inflammatory/analgesic (Carprofen, 5 mg/kg). After surgery, the rats were allowed 7 days of recovery before the experiment began. They were then placed on a food deprivation schedule that kept them at 90% of their free-feeding body weight.

**Apparatus**. The 2- and 4-connected-rooms environments were derived from a 150 x 150 cm square arena with 60 cm high grey walls and covered with a gray vinyl sheet that can be wiped with a moistened sponge to neutralize smells. The apparatus was isolated from the rest of the room by an opaque circular curtain 260 cm in diameter. Ceiling lights lighted the environments homogeneously and a radio fixed to the ceiling above the environments was used to mask uncontrolled directional sounds. The unit recording system and equipment for controlling the experiment were in an adjacent room.

To create a two visually identical opposite connected rooms, we divided the arena in 2 equal rectangular rooms (75 x 150 cm) by inserting a 60 cm high wall with a door at the center (an aperture of 10 cm at the base and 15 cm at the top) (**Figure 1A and Supplementary figure**

**1A**). For the four visually identical orthogonal connected rooms, we divided the arena in four equal square rooms (75 x 75 cm) by inserting two 60 cm high walls perpendicularly, each having two doors allowing to connect each room with the two adjacent ones (**Figure 2A and Supplementary figure 1B**). We polarized each room with identical white cue cards (30 x 40 cm, one per room) attached to the opposite short walls in the 2-identical-rooms environment, or to the orthogonally arranged walls in the 4-identical-rooms environment. To maximize the difference between the rooms, in the 2- and 4-different-rooms environments, each cue card had a specific pattern (a circle, stripes, a square, a star, a triangle) and each floor was covered with vinyl of different texture and visual pattern (**Supplementary figure 1C and D**).

**Recording setup.** Both screening and recordings were performed in the experimental room. A counterbalanced cable was attached at one end to an automatic commutator and at the other end to the headstage containing a field effect transistor amplifier for each tetrode wire. The signals from each tetrode wire were amplified 10 000 times, bandpass filtered between 0.3 and 3 kHz with Neuralynx amplifiers (Neuralynx, Bozeman, MT, USA), digitized (32 kHz), and stored by DataWave Sciworks acquisition system (DataWave Technologies, Longmont, CO, USA). Two light-emitting diodes (LED), one red and one green attached to the headstage provided the position and the orientation of the rat's head. The LEDs were imaged with a CCD camera fixed to the ceiling above the maze, and their position was tracked at 25 Hz with a digital spot-follower. A food dispenser of 20 mg food pellets was located 2 m above the environment. Animals were moving freely while food was randomly dropped on the floor to motivate them to explore the entirety of the environment.

**Recording protocols**. Recordings began one week after the surgery. The animals were daily screened in an individual box to identify single unit activity. When no single unit was observed or after a completed recording protocol, the tetrodes were lowered 50 µm. When one or several units were isolated, we started one of the 3 recording protocols of the study:

1. one session in the 2-identical-connected-rooms environment followed by one session in the 2-different-connected-rooms environment.
2. one session in the 4-identical-connected-rooms environment followed by one session in the 4-different-connected-rooms environment.
3. one session in the 2-different-connected-rooms environment followed by one session in the 4-different-connected-rooms environment.

Each session lasted 10-20 minutes, and the floor was cleaned between sessions and at the end of the protocol. Between successive sessions, the rats were not disconnected but were removed from the apparatus and placed in a random location in an individual box to let the experimenter manipulate the apparatus (changing the visual cues, the floors and/or the central walls, cleaning the walls and the floor). Animals were then mildly disoriented by rotating the box before the next session.

**Data analyses**. All data analyses (except for the spike sorting) were performed with Matlab® custom scripts.

***Spike sorting.*** Spike sorting was performed manually using the graphical cluster-cutting software Offline Sorter (Plexon). Units selected for analysis had to be well-discriminated clusters with spiking activity clearly dissociated from background noise. Units having inter-spike intervals < 2 ms (refractory period), were removed due to poor isolation. To prevent

repeated recordings of the same cell over days, clusters that recurred on the same tetrodes in the same cluster space across recording sessions were only analyzed one time.

***Directionality analyses.*** The rat's head direction was calculated for each tracker sample from the projection of the relative position of the two LEDs onto the horizontal plane. The directional tuning for each cell was obtained by dividing the number of spikes when the rat faced a particular direction (in bins of 6°) by the total amount of time the rat spent facing that direction. The cell's PFD is the circular mean of the directional tuning. Further analyses were only performed on cells having a peak firing rate exceeding 1 Hz.

***Direction cells selection.*** To assess the directional specificity of **HDCs,** the Rayleigh vector length was used, with significant directionality being assigned to cells whose Rayleigh vector score exceeded 0.2. **Bidirectional cells** (**BDCs)** were identified with a flip score exceeding 0.6, as in a previous study in which it was necessary to select BDCs (*Jacob et al. 2017*). The flip score was calculated with an autocorrelation procedure, by rotating the polar firing rate plot in steps of 6° and calculating the correlation between the rotated and unrotated plots at each step. The flip score for each cell was defined as the difference between the correlations at the expected peak (180°) and the expected trough (90°). **MDCs** were defined as cells showing multidirectional activity in the 4-connected-rooms environment but showing unipolar activity in individual rooms. MDCs were selected based on one criterion: the Rayleigh vector score calculated from the directional activity in each of the four rooms had to exceed 0.2 in at least one of the four rooms.

***Stability of the BDCs and HDCs activities.*** We assessed the stability of BDCs and HDCs by comparing the flip score of BDCs and the Rayleigh vector length of HDCs between the 2-

identical- and the 2-different-connected-rooms environments. Then, for each BDC and HDC we computed the circular correlation between the directional firing in the 2-identical- and 2-different-connected-rooms environments. From this we extracted the maximum correlation coefficient and the corresponding angle. The distribution of all angles was then computed for all BDCs and HDCS separately, and the Rayleigh test was used to test its uniformity and to calculate the mean circular direction. For the correlation coefficients, we calculated the mean values separately for BDCs and HDCs and tested whether it significantly differed from 0 using either a one-sample t-test or a one-sample Wilcoxon test.

***Characterization of the MDCs activity.*** We calculated the Rayleigh vector length and the PFD in each room, and we compared their values between the 4-identical- and 4-different-connected-rooms environments using a two-way ANOVA (with environments and rooms as main factors). Since the rooms in the 4-connected-rooms environments are arranged orthogonally, we tested whether the PFDs were separated by 90° between rooms. For each cell, we calculated the differences between the PFDs of any two adjacent rooms and tested whether they were distributed around 90°, extracting the circular mean value and the corresponding angle. Finally, we tested the multidirectional stability between the 4-identical and 4-different-connected-rooms using the same procedure as for BDCs and HDCs activity (previous section).

***Comparison between 2-different and 4-different-connected-rooms environments.*** We analyzed whether cells changed their activity between 2- and 4-different-connected-rooms environments by comparing the peak firing rate and either the flip scores or the vector lengths, respectively for BDCs and HDCS, using a repeated measure ANOVA. Then, we assessed the stability of HDCs and BDCs between rooms or sessions as previously described.

***Spatial ratemaps and place cell selection***. Spatial ratemaps were generated by dividing the environment into square bins, each 2.5 × 2.5 cm in size. Spikes per bin were divided by the time spent in that bin to provide a raw firing ratemap. Smoothed firing ratemaps were then generated using a boxcar procedure in which the firing rate in each bin was replaced by that of the mean of itself plus the immediately surrounding bins. The firing rate of the cell was color-coded from low (light blue) to high (dark red). In both raw and smoothed ratemaps, pixels that were not visited by the rat were displayed in white.

For each map, we calculated two classical measures of spatial selectivity:

- the spatial coherence as the spatial autocorrelation of the non-smoothed place field and measures the extent to which the firing rate in a particular bin is predicted by the average rate of the eight surrounding bins.

- the spatial information content, expressed in bits per spike and is calculated as follows:

$$I = i \sum P(i) \left( \frac{\lambda i}{\lambda} log_2 \frac{\lambda i}{\lambda} \right)$$

Where $P(i)$ is the occupancy probability of bin, $\lambda i$ is the mean firing rate in bin and $\lambda$ is the overall mean firing rate.

Hippocampal cells were categorized as place cells if they satisfied 4 criteria in at least one room of the 2- or 4-connected-rooms environments:

1- the place field should include at least nine contiguous pixels of the non-smoothed ratemap with a firing rate above the mean firing rate (averaged over the environment).

2- the peak firing rate should exceed 1Hz.

3- the spatial coherence score should exceed 0.4.

4- the spatial information content should exceed 1.

***Spatial correlation.*** To analyze whether both place cells and RSC neurons have repeated, opposite or unrelated spatial activity between rooms, we constructed for each cell the ratemaps in each separated room. For the 2-connected-rooms environments, we calculated the Pearson product-moment correlation coefficient on Fisher-transformed values between the 2 non-smoothed spatial ratemaps either unchanged or rotated by 180°, to match the position of the door and the visual cue cards. For the 4-connected-rooms environments, we calculated all possible spatial correlations between any two rooms (4 correlations for adjacent rooms and 2 correlations for opposite rooms) which we either averaged altogether, or averaged according to whether the rooms were adjacent or opposite. In order to assess whether place fields rotated or repeated across rooms, we calculated the mean spatial correlation of the unchanged rooms and after rotating three of the four rooms by 90°, -90° and 180° in order to overlap the position of the doors and the visual cue cards.

Finally, we tested whether place cell activity changed between multicompartment environments with identical and different rooms by calculating the spatial correlation between 2-identical and 2-different-connected-rooms environments as well as between 4-identical and 4-different-connected-rooms environments.

**Statistical analyses**. Statistics were performed with GraphPad Prism 9® and included Mann-Whitney U test, one-sample Wilcoxon test, one-sample Student's t-test, two-samples Student's t-test either paired or unpaired, one-way ANOVA, two-way ANOVA and repeated-measure ANOVA, Tukey's post hoc, were performed when allowed. Rayleigh tests for uniformity and circular V-tests were performed with Matlab®.

**Histology**. At the completion of the experiment, after induction of deep sedation (Domitor, 500µg/kg) rats received an overdose of barbiturate (Euthasol, 200 mg/kg). The brains were removed and frozen with isopentane cooled at -80°C. Then 25 µm-thick coronal sections were mounted on glass slides (SuperFrost Plus®, ThermoFisher) and stained with thionine. The position of the tips of the electrodes was determined from digital pictures, acquired with a Leica Microscope (Wetzlar, Germany), and imported in an image manipulation program (Gimp 2.8, distributed under General Public License). Delimitations of the RSC were based on Paxinos and Watson's stereotaxic atlas (*Paxinos & Watson, 2007*), recording sites were determined by measuring backwards from the deepest point of the track.

# Results

**BDCs and HDCs maintain directional activity in the 2-visually-different-connected-rooms environment.**

A previous study has described the properties of the RSC BDCs firing in two opposite directions in two visually symmetrical connected rooms having different odors (*Jacob et al., 2017*). To investigate how local and global reference frames influence BDCs and HDCs, we implanted recording electrodes in the dysgranular RSC (**Supplementary figure 2**). We first identified both BDCs and HDCs in a 2-visually-symmetrical-connected-rooms environment (S1-2id) but without any odor cues as the original experimental setup. Then, animals were exposed to an environment made of 2-visually-different-connected-rooms (S2-2dif) (**Figure 1A**). Among 1206 RSC neurons recorded in 9 rats we identified **30** BDCs (**Figure 1B-C**) and **77** HDCs **(Figure 1D-E)**. The Rayleigh test showed no significant clustering of the PFDs, indicating that both BDCs and HDCs represent the entire range of 360° directions (**Supplementary figure 3**;

Rayleigh test for BDCs, Z = 0.45, p = 0.64; Rayleigh test for HDCs, Z = 0.62, p = 0.54). These results indicate that odors are not critical for BDCs and HDCs firing.

We then compared the activity of **26** BDCs and **40** HDCs between S1-2id and S2-2diff. We found similar flip scores between the two environments (**Figure 1F**: mean S1-2id = 0.94±0.34, mean S2-2diff = 0.77±0.43, unpaired t-test, t(54) = 1.62, p = 0.11), although 6 BDCs lost their bidirectional pattern in S2-2diff. BDCs maintained a similar double angle vector length (**Supplementary figure 4**; mean S1-2id = 0.29±0.08, mean S2-2diff = 0.25±0.01, unpaired t-test, t(54) = 1.53, p = 0.13) and peak firing rate (**Figure 1F**: mean S1-2id = 4.54±4.05, mean S2-2diff = 3.77±2.90, unpaired t-test, t(54) = 0.81, p = 0.42). As in S1-2id, in S2-2diff the BDCs show directional activity uniformly distributed around the 360° directions (**Supplementary figure 3;** Rayleigh test, Z = 1.27, p = 0.28). We then tested the stability of BDCs between S1-2id and S2-2diff by computing the circular correlation of BDCs firing by step of 6°, from which we extracted the maximum correlation values and their corresponding angles. The mean correlation value was significantly greater than 0 (**Figure 1G left panel** mean = 0.67±0.13, one sample t-test on Fisher-transformed values, t(25) = 25.58; p < 0.0001), and angles at maximum correlation were clustered close to 0° (**Figure 1G right panel**; mean vector length, VL = 0.72; mean direction, dir = 4°; V-test for 0°, V = 18.83, p < 0.001), indicating that bidirectional activities are stable between S1-2id and S2-2diff.

Similar results were obtained for the 40 HDCs recorded in S1-2id and S2-2diff. The Rayleigh vector length (mean S1-2id = 0.29±0.11, mean S2-2diff = 0.33±0.19) and peak firing rate (mean S1-2id = 9.46±22.35, mean S2-2diff = 7.06±10.78) did not change between the two environments (**Figure 1H:** unpaired t-test for Rayleigh vector length, t(115) = 1.23, p = 0.22; unpaired t-test for peak firing rate, t(115) = 0.64, p = 0.52) and directional activities are uniformly distributed (**Supplementary figure 3;** Rayleigh test, Z = 0.79, p = 0.46). HDCs

displayed great stability between S1-2id and S2-2diff, although 5 of them lost their directional activity in S2-2diff. The mean of correlation value between S1-2id and S2-2diff is significantly greater than 0 (**Figure 1I left panel**; mean value = 0.74±0.19, one sample t-test on Fisher-transformed values, $t(39) = 23.79$; $p < 0.0001$) and the distribution of angles at maximum correlation were clustered close to 0° (**Figure 1I right panel**; mean vector length, VL = 0.71; mean direction, dir = -7°; V-test for 0°, V = 28.32, $p < 0.001$).

Altogether, these results indicate that the visual ambiguity caused by the two identical rooms is not likely to generate BDCs firing but rather depends on the structure of the environment. This supports the hypothesis that BDCs and HDCs are anchored to local and global reference frames, respectively. This is also supported by simultaneous recordings of both BDCs and HDCs in S1-2id and S2-2diff (**Supplementary figure 5**).

**Figure 1**

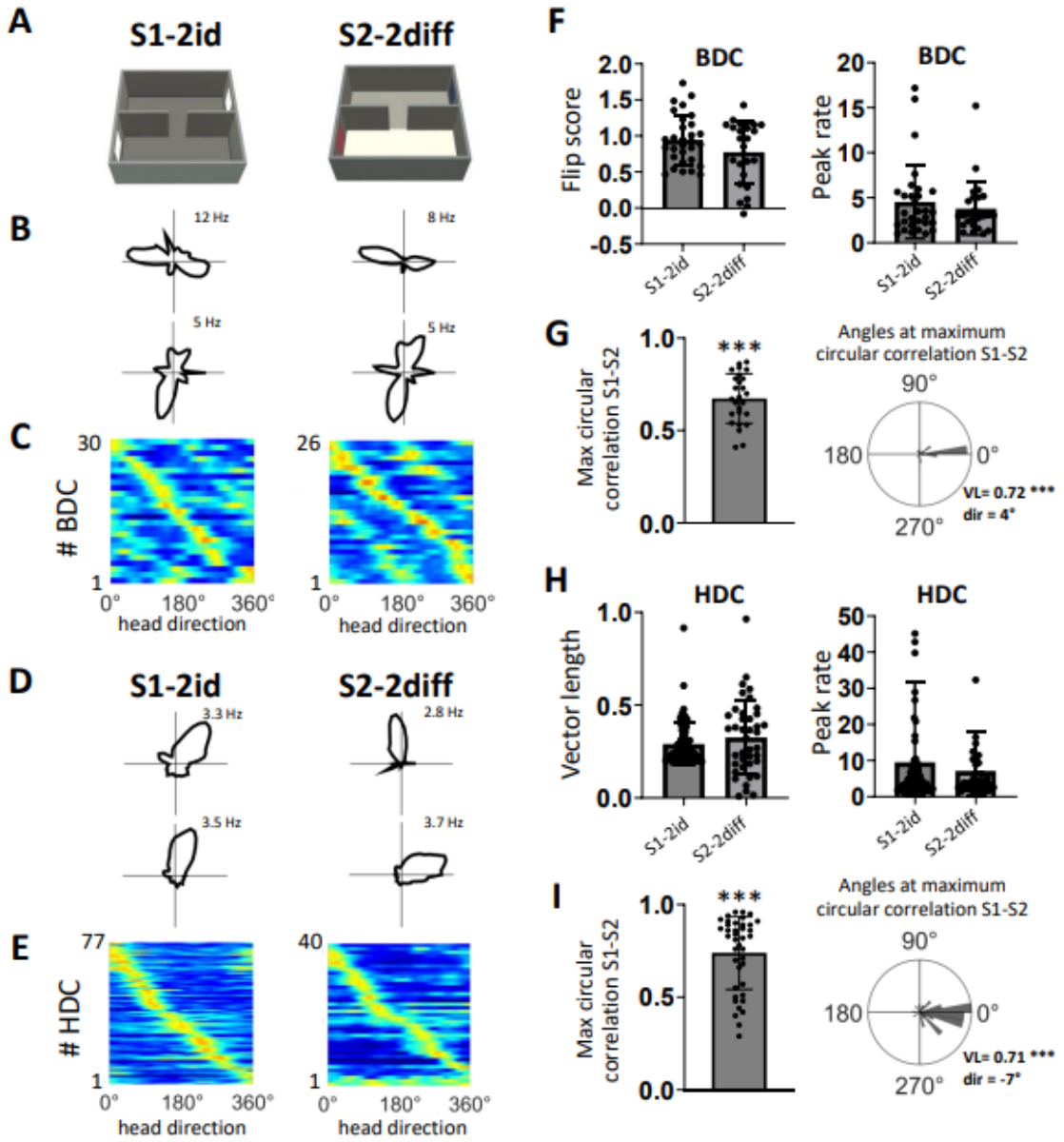


**Figure 1. Bidirectional and head direction firings are maintained between 2-identical and 2-different-connected-rooms. A.** Animals successively explored two environments consisting of 2-connected-rooms either identical (S1-2id: same visual cue and floor) or different (S2-2diff: different visual cues and different floors). **B.** Example of 2 BDCs recorded in the two environments (top and bottom). For each cell, the peak firing rate is indicated. **C.** Directional activity of 30 BDCs recorded in S1-2id (left); among them, 26 BDCs were successively recorded in S2-2diff (right). Activity is color-coded from blue (no activity) to orange (peak

firing rate) and BDCs are sorted according to their PFD. **D.** Example of 2 HDCs recorded in the two environments (top and bottom); the peak firing rate is indicated. **E.** Color-coded directional activity of 77 HDCs recorded in S1-2id (left); among them 40 HDCs were successively recorded in S2-2diff (right). HDCs were sorted according to their PFD. **F.** Mean flip score (left) and peak rate (right) of BDCs in S1-2id and S2-2diff. **G.** Left: The mean of maximum circular correlation values of BDCs activity between the two environments is significantly greater than 0. Right: The angles at maximum correlation values are clustered near 0° (dir = 4°). **H.** Mean vector length (left) and peak rate (right) of HDCs in the two environments. **I.** As for the BDCs, HDCs show both an average maximum circular correlation value greater than 0 and a distribution of the corresponding angles clustered near 0° (dir = 7°). Individual data are represented by black dots. VL: vector length; dir: mean value of angle distributions. *** $p < 0.001$ One sample t-test and Rayleigh test.

**RSC neurons show multidirectional activity in 4-connected-rooms environments.**

To test the 'local-global reference frames' hypothesis, we recorded RSC cells activity in both 4-visually-identical-connected rooms (S1-4id) and 4-visually-different-connected-rooms (S2-4diff) environments (**Figure 2A**). According to this hypothesis, we should expect some cells to show multidirectional activity. To select MDCs, we computed the Rayleigh vector length of cells directional activity in each room. Cells having a vector length above 0.2 at least in one room were selected as putative MDCs. Over 3 rats, we identified **22** MDCs in S1-4id, and among them we followed the activity of **11** MDCs in S2-4diff (**Figure 2B-C-D**). The distribution of PFDs represents all the 360° directions (**Figure 2D;** Rayleigh test for S1-4id, Z = 0.23, p = 0.80; S2-4diff, Z = 0.43, p = 0.80). Visual inspection of the MDCs' directional tuning curves in figure 2B shows a tetradirectional activity in S1-4id that tends to become bidirectional in S2-4diff. However, it is possible that such bidirectional activity is indeed tetradirectional, with two firing directions overshadowing the two others. We thus constructed the head direction activity in each room (**Figure 2C**) and observed that MDCs show a unipolar

activity resembling a ‘classical’ HDC activity. We thus compared vector lengths and peak rates of MDCs between rooms (**Figure 2E-F**). The two-way ANOVA shows a room effect for both vector length and peak rate, but no environment S1-4id x S2-4diff effect and no interaction between the two factors (two-way ANOVA, vector length: room effect, $F(3,93) = 3.36$, $p = 0.02$; environment S1-4id x S2-4diff effect, $F(1,31) = 0.11$, $p = 0.74$; environment x room effect, $F(3,93) = 1.88$, $p = 0.14$; peak rate: room effect, $F(3,93) = 5.08$, $p = 0.003$; environment effect, $F(1,31) = 0.28$, $p = 0.60$; environment x room effect, $F(3,93) = 1.82$, $p = 0.15$). We then calculated for each MDC the difference between the PFDs in the 4 rooms for both S1-4id and S2-4diff (**Figure 2G**). The distribution of these differences show that MDCs have orthogonal PFDs between rooms (S1-4id: mean vector length, VL = 0.64; mean direction, dir = 95°; $Z = 36.45$, $p < 0.001$; S2-4diff: mean vector length, VL = 0.54; mean direction, dir = 90°; $Z = 13.11$, $p < 0.001$), indicating that MDCs firing is tetradirectional in the 4-rooms environments.

Finally, we analyzed the circular correlation of MDCs activity between S1-4id and S2-4diff (**Figure 2H left panel**). The median of the correlation coefficient was significantly greater than 0 (median value = 0.57; one sample Wilcoxon test on Fisher-transformed values, $W = 66$, $p = 0.001$). Moreover, the distribution of angles at maximum correlation are clustered close to 0° (**Figure 2H right panel**; mean vector length, VL = 0.96; mean direction, dir = 8°; V-test for 0°, $V = 10.53$, $p < 0.001$). These results indicate that the RSC possesses neurons having multidirectional firing in 4-different-connected-rooms.

Figure 2

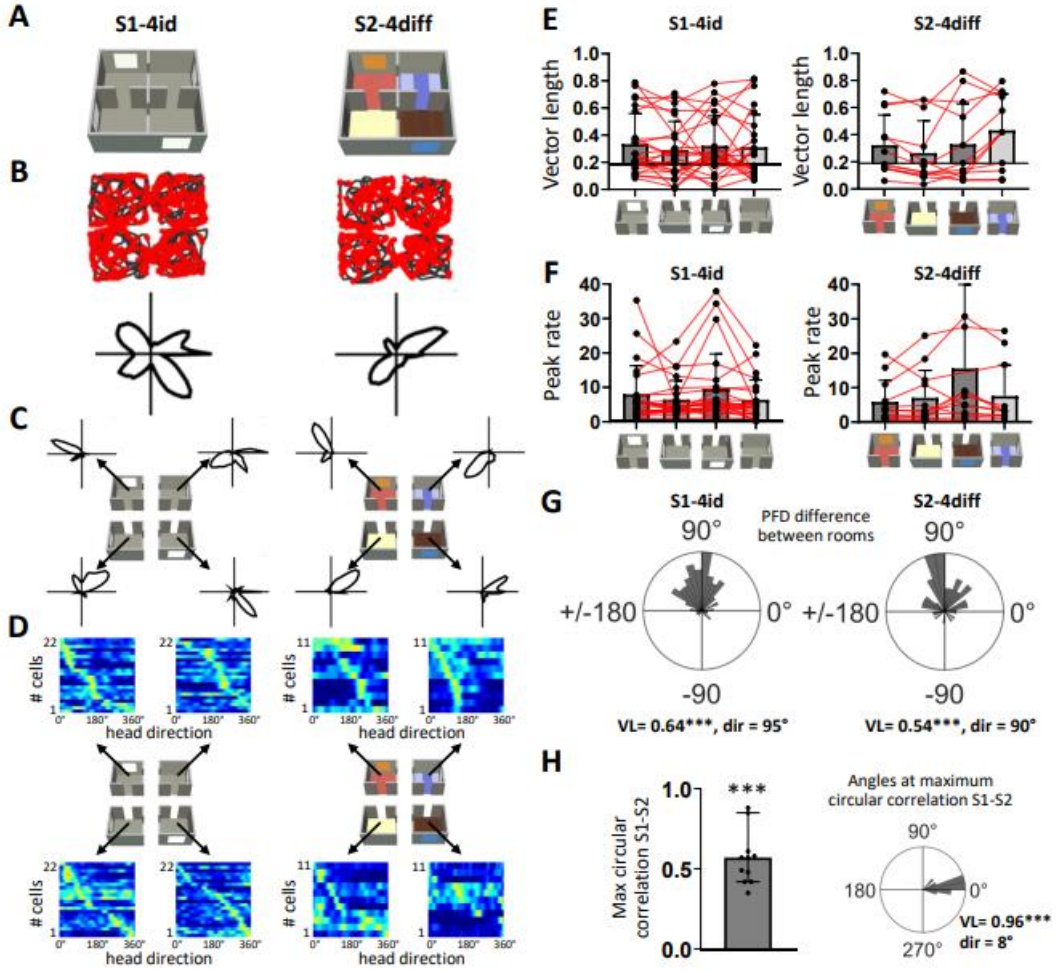


**Figure 2. Multidirectional firing in a 4 rooms environment. A.** Animals successively explored two environments consisting of 4-connected-rooms either identical (S1-4id: same visual cue and floor) or different (S2-4diff: different visual cues and different floors). **B.** Example of one MDC recorded in the two environments. Top: Action potentials (red dots) superimposed on the animal's path (black). Bottom: polar plot of the firing rate *vs* head direction. **C.** Tuning curve of a MDC activity for each room separately. **D.** Directional activity in each room for 22 MDCs recorded in S1-4id (left); among them, 11 MDCs were successively recorded in S2-4diff (right). MDCs have unipolar activity in each room. **E-F.** Mean vector length (E) and peak rate (F) of MDCs in each room of the S1-4id and S2-4diff environments. **G.** The polar distribution of PFD differences between rooms shows that MDCs have PFD shifted by 90° from one room to the other, in both S1-4id and S2-4diff. **H.** MDCs maintain a stable multidirectional pattern between S1-4id and S2-4diff. The mean of maximum circular

correlation values of MDCs activity between the two environments is significantly greater than 0 (left). The distribution of the corresponding angles is clustered near 0° (dir = 8°). Individual data are represented by black dots. VL: Vector length; dir: mean direction of distribution. *** $p < 0.001$, Rayleigh test and one sample Wilcoxon test.

**BDCs in 2-different-connected-rooms become MDCs in the 4-different-connected-rooms environments.**

We next investigated whether MDCs and BDCs are the same population of neurons, in two additional rats. We identified 42 BDCs in the 2-different-connected-rooms (S1-2diff) and followed the activity of 32 of them in the 4-different-connected-rooms (S2-4diff) (**Figure 3A**). Rayleigh tests on BDCs PFDs showed no significant clustering in both S1-2diff and S2-4diff, indicating that BDCs represent the entire range of 360° directions (**Supplementary figure 3**; Rayleigh test for S1-2diff, Z = 0.87, p = 0.42; Rayleigh test for S2-4diff, Z = 1.41, p = 0.25). **Figure 3A** shows examples of 2 BDCs recorded in S1-2diff that become multidirectional in S2-4diff. The drop of the flip score in S2-4diff indicates that BDCs loose the bidirectional pattern in the 4-different-connected-rooms environment (mean S1-2diff = 0.91±0.27, mean S2-4diff = -0.07±0.42, unpaired t-test, t(72) = 11.97, p < 0.001), while the peak firing rate does not change (mean S1-2diff = 5.32±4.85, mean S2-4diff = 4.36±4.10, unpaired t-test, t(72) = 0.90, p = 0.37) (**Figure 3B**). Then we asked whether BDCs show unipolar activity within each room in S1-2diff and S2-4diff. **Figure 3C** show examples of the directional activity of two BDCs in each room, for both S1-2diff and S2-4diff environments. Both BDCs show clear unipolar activity in each room of the S2-4diff environment, even if the multidirectional pattern is not clearly evident from the global polar plot (see the example of BDC 4). **Figure 3D-E** shows the directional activity of all BDCs in each room, sorted by direction. All BDCs have significant

unipolar activity in each room of the S1-2diff environment (**Supplementary figure 6**; S1-2diff, mean vectors length, room 1 = 0.22±0.16, room 2 = 0.22±0.15, paired t-test, t(41) = 0.10, p = 0.92). We observed same results for BDCs in S2-4diff (**Supplementary figure 6**; S2-4diff, mean vectors length, room 1 = 0.30±0.20, room 2 = 0.28±0.16, room 3 = 0.29±0.19, room 4 = 0.33±0.22, one-way ANOVA, F(2.492,77.25) = 0.73, p = 0.51).

We also calculated for each BDC the PFD difference between the 2 or 4 rooms for S1-2diff and S2-4diff respectively (**Figure 3F**). The distribution of the differences shows that BDCs have opposite PFDs between rooms in S1-2diff and orthogonal PFDs between rooms in S2-4diff (S1-2diff: mean vector length, VL = 0.40; mean direction, dir = 170°; Z = 6.63, p = 0.001; S2-4diff: mean vector length, VL = 0.43; mean direction, dir = 83°; Z = 24.18, p < 0.001), indicating that BDCs firing becomes tetradirectional in the 4-connected-rooms environment.

Finally, circular correlations of BDCs activity between S1-2diff and S2-4diff shows a median correlation value (0.47) significantly greater than 0 (one sample Wilcoxon test on Fisher-transformed values, W = 528; p < 0.001) (**Figure 3G left panel**). The distribution of angles at maximum correlation values between S1-2diff and S2-4diff is clustered near 0°, -90° and 180°, with only -90° being significant for the circular V-test (mean vector length, VL = 0.24; mean direction, dir = 87°; V-test for 0°, V = 0.46, p = 0.45; V-test for -90°, V = 7.56, p = 0.03; V-test for 180°, V = -0.46, p = 0.55) (**Figure 3G right panel**). Altogether, these results indicate that BDCs become MDCs when increasing the number of different connected rooms from 2 to 4.

We used same analysis for the RSC HDCs (**Figure 3H**). We recorded 145 HDCs in S1-2diff and we followed the activity of 113 of them in S2-4diff. Few HDCs were recorded simultaneously with BDCs in both S1-2diff and S2-4diff (**Supplementary figure 5**). We observed no differences of the vector lengths (**Figure 3I left panel:** mean S1-2diff = 0.45±0.24, mean S2-4diff = 0.46±0.23, unpaired t-test, t(256) = 0.62, p = 0.53) nor the peak firing rate

(**Figure 3I right panel:** mean S1-2diff = 17.54±23.94, mean S2-4diff = 16.87±24.57, unpaired t-test, $t(256) = 0.22$, $p = 0.83$). The PFDs of HDCs are uniformly distributed around 360° in S2-4diff (**Supplementary figure 3**; Rayleigh test for S2-4diff, $Z = 0.37$, $p = 0.69$) but not in S1-2diff (**Supplementary figure 3**; Rayleigh test for S1-2diff, $Z = 3.21$, $p = 0.04$). Consistently with well-established HDCs properties, the PFDs remain stable in the different rooms of both environments (**Figure 3J-L**), with similar vector length between the rooms and between environments (**Supplementary figure 6**; mean S1-2diff, room 1 = 0.47±0.24, room 2 = 0.45±0.25, paired t-test, $t(144) = 1.27$, $p = 0.21$; mean S2-4diff, room 1 = 0.50±0.26, room 2 = 0.46±0.26, room 3 = 0.51±0.26, room 4 = 0.51±0.26, one-way ANOVA, $F(2.38,266.9) = 1.68$, $p = 0.18$). The distribution of PFD differences between rooms confirms that HDCs maintains the same PFD across connected rooms in both S1-2diff and S2-4diff (**Figure 3M**: S1-2diff: mean vector length, VL = 0.74; mean direction, dir = 5°; $Z = 79.89$, $p < 0.001$; S2-4diff: mean vector length, VL = 0.63; mean direction, dir = 8°; $Z = 177.93$, $p < 0.001$).

Finally, PFDs remain stable between S1-2diff and S2-4diff (**Figure 3N left panel**: mean of correlation = 0.88±0.11, one sample t-test on Fisher-transformed values, $t(79) = 70.38$, $p < 0.0001$) (**Figure 3N right panel:** mean vector length, VL = 0.48; mean direction, dir = 5°; V-test for 0°, $V = 38.37$, $p < 0.001$), confirming that HDCs are not affected by environmental changes nor by the number of connected rooms (*Jacob et al., 2017; Lozano et al., 2017; Zhang et al., 2022*).

## Figure 3

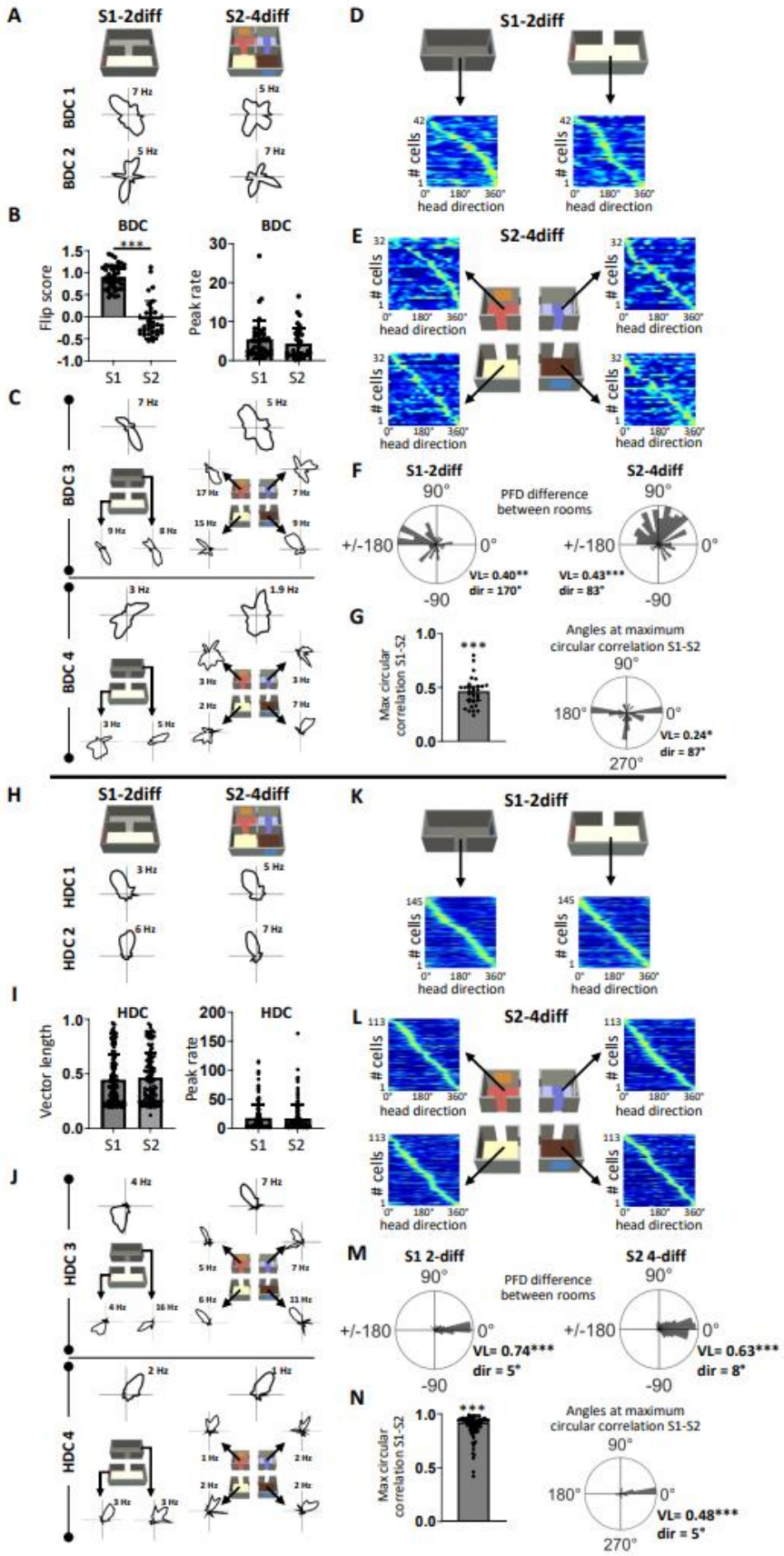
A
S1-2diff
S2-4diff
BDC 1
BDC 2
B
BDC
Flip score
Peak rate
S1
S2
C
BDC 3
BDC 4
D
S1-2diff
# cells
head direction
E
S2-4diff
F
S1-2diff
S2-4diff
PFD difference between rooms
VL= 0.40**
dir = 170°
VL= 0.43***
dir = 83°
G
Max circular correlation S1-S2
Angles at maximum circular correlation S1-S2
VL= 0.24*
dir = 87°
H
S1-2diff
S2-4diff
HDC 1
HDC 2
I
HDC
Vector length
Peak rate
J
HDC 3
HDC 4
K
S1-2diff
L
S2-4diff
M
S1 2-diff
S2 4-diff
PFD difference between rooms
VL= 0.74***
dir = 5°
VL= 0.63***
dir = 8°
N
Max circular correlation S1-S2
Angles at maximum circular correlation S1-S2
VL= 0.48***
dir = 5°

**Figure 3. Bidirectional cells in a 2-rooms environment become tetradirectional in a 4-rooms environment. A.** Top: Animal successively explored two environments made of 2-different-connected-rooms (S1-2diff) and 4-different-connected-rooms (S2-4diff). Middle & bottom: polar plot of firing rate *vs* head direction of 2 BDCs (BDC1 and BDC2) in S1-2diff and S2-4diff. **B.** The mean flip score (left) of BDCs significantly decreases in the 4 rooms environment, while the mean peak rate (right) does not change between the two environments. **C.** Example of the tuning curves of two BDCs (BDC3 and BDC4) for each room separately reveals that BDCs have unipolar activity in each room regardless of the number of connected rooms. **D-E.** Directional activity in each room of 42 BDCs recorded in S1-2diff (top). Among them, 32 were successively recorded in S2-4diff, where they became MDCs (bottom). All cells show unipolar activity in each room. **F.** Polar distributions of PFD differences between rooms in S1-2diff and S2-4diff. Distributions are opposite in the 2 rooms environment (Vector length (VL) = 0.40*** and mean direction (dir) = 170°) and orthogonal in the 4 rooms environment (Vector length (VL) = 0.43*** and mean direction (dir) = 83°). **G.** BDCs activity between S1-2diff and S2-4diff are shifted by multiples of 90°. The mean of maximum circular correlation values of BDCs activity between the two environments is significantly greater than 0 (left). The distribution of corresponding angles is clustered around orthogonal values (right). **H.** Example of polar activity of 2 HDCs (HDC1 and HDC2) in S1-2diff and S2-4diff. **I.** The mean vector length (left) and peak rate (right) of HDCs do not change between S1-2diff and S2-4diff. **J-K-L.** HDCs maintain unipolar activity between connected rooms. (J) Examples of the tuning curves of two HDCs (HDC3 and HDC4) for each room separately. (K-L) Directional activity in each room of 145 HDCs in S1-2diff (K); among them, 113 HDCs were also recorded in S2-4diff (L). **M.** HDCs maintain the same PFD between rooms as shown by polar distributions of the PFD differences between rooms in S1-2diff (left) and S2-4diff (right), respectively. Both distributions are clustered near 0° (5° and 8° respectively) **N.** HDCs activity is stable between S1-2diff and S2-4diff. The mean of the maximum circular correlation values between S1-2diff and S2-4diff is significantly greater than 0 (left) and the corresponding angles are clustered near 0° (dir = 5°; right) (right). Peak frequencies are indicated for polar plots; individual data are represented by black dots; VL: vector length; dir: mean value of angle distributions. *** $p < 0.001$, Two sample, one sample t-test, one sample Wilcoxon test and Rayleigh test.

**RSC encodes spatial information anchored to features of the rooms.**

The RSC has been shown to provide a spatial code for a particular context at single-cell level (*Alexander et al., 2015, 2017; Mao et al., 2017, 2018; Milczarek et al., 2018; Miller et al., 2019, 2021; Vedder et al., 2016; Xie et al., 2014*). In our study each room may provide a single context. We therefore asked whether the RSC neurons encode this type of spatial information. For each cell that were not directional (neither a HDC nor a BDC nor a MDC), we constructed the spatial ratemap for each room, and we calculated the spatial correlation between the rooms, either unrotated or rotated to overlap the position of the door and visual cues. We hypothesized to observe 3 possible results (**Figure 4A and 5B**): 1) a spatial pattern oppositely and orthogonally repeated respectively in 2- and 4-connected-rooms environments; 2) a spatial pattern identically repeated in all rooms, irrespective of the environment; and 3) a different spatial pattern in each room. For both 2-identical (S1-2id) and 2-different-connected-rooms (S2-2diff) environments, we recorded 222 non-directional cells and observed greater mean spatial correlation for rotated ratemaps compared to unrotated ratemaps, the latter having a mean correlation value close to 0 (**Figure 4B-E**). Repeated measure ANOVA shows a unrotated/rotated ratemap effect ($F(1,221) = 71.51$, $p < 0.0001$), an identic/different rooms effect ($F(1,221) = 4.24$, $p = 0.041$) and no interaction ($F(1,221) = 0.82$, $p = 0.37$). Tuckey's post hoc confirm the significantly greater spatial correlation for rotated ratemaps compared to unrotated ones (S1-2id and S2-2diff, $p < 0.0001$). These results suggest that RSC neurons encode spatial information that is oppositely repeated in 2-connected-rooms environments.

Figure 4

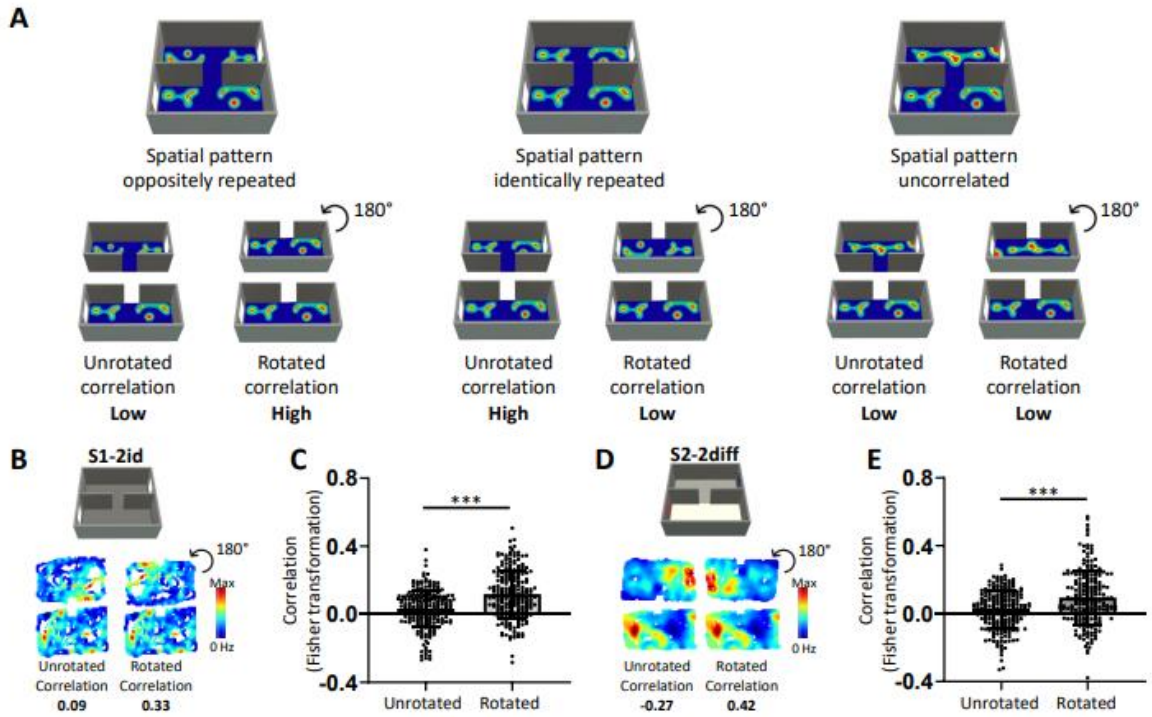


**Figure 4. RSC neuron spatial activity is oppositely repeated between 2-connected-rooms. A.** Three hypothetical spatial patterns in the 2-connected-rooms environments (top) and the corresponding spatial correlation (either low or high). **B-D.** Examples of spatial ratemaps in the 2-identical-connected-rooms (B – S1-2id) and in the 2-different-connected-rooms (D – S2-2diff) environments showing repeated and opposite spatial patterns. **C-E.** The average of spatial correlation values is significantly greater for rotated ratemaps than for unrotated ratemaps, regardless of whether connected rooms are identical or different (n = 222). Individual data are represented by black dots. *** $p < 0.001$, Repeated measure ANOVA.

For the 4-connected-rooms environments, we performed the same analysis on 76 cells recorded in 4-identical (S1-4id) and 4-different-rooms (S2-4diff) environments (**Figure 5**). Similarly to 2-connected-rooms environments, the average spatial correlation is significantly greater for rotated ratemaps compared to unrotated ratemaps, the latter having a mean correlation value close to 0 (**Figure 5C-D and 5F-G**). The repeated measure ANOVA shows a significant

unrotated/rotated ratemap effect ($F(1,75) = 86.88$, $p < 0.0001$), no identic/different rooms effect ($F(1,75) = 0.08$, $p = 0.78$), and no interaction ($F(1,75) = 3.91$, $p=0.052$). These results indicate that in 4-connected-rooms environments RSC neurons encode spatial information that is orthogonally repeated. To confirm this, we separated the maps from opposite and adjacent rooms. Since opposite rooms have 180° symmetry, we should expect the rotated maps to be positively correlated and the unrotated maps to be anti-correlated. As for the adjacent rooms, having a 90°-degree symmetry, rotated maps should be positively correlated while unrotated maps should have no correlation. For both S1-4id and S2-4diff environments the repeated measure ANOVA shows an adjacent/opposite rooms effect (S1-4id: $F(1,75) = 53.84$, $p < 0.0001$; S2-4diff: $F(1,75) = 34.49$, $p < 0.0001$), an unrotated/rotated ratemap effect (S1-4id: $F(1,75) = 71.21$, $p < 0.0001$; S2-4diff: $F(1,75) = 89.15$, $p < 0.0001$) and an interaction (S1-4id: $F(1,75) = 31.62$, $p < 0.0001$; S2-4diff: $F(1,75) = 37.78$, $p < 0.0001$) (**Figure 5E and 5H**). Tukey's post hoc confirms that the correlation between unrotated ratemaps is significantly lower for opposite rooms compared to adjacent rooms, while no differences is observed between opposite and adjacent rooms for rotated ratemaps.

Overall, these results confirm that non-directional RSC neurons support spatial information that is anchored to spatial features of the rooms.

Figure 5

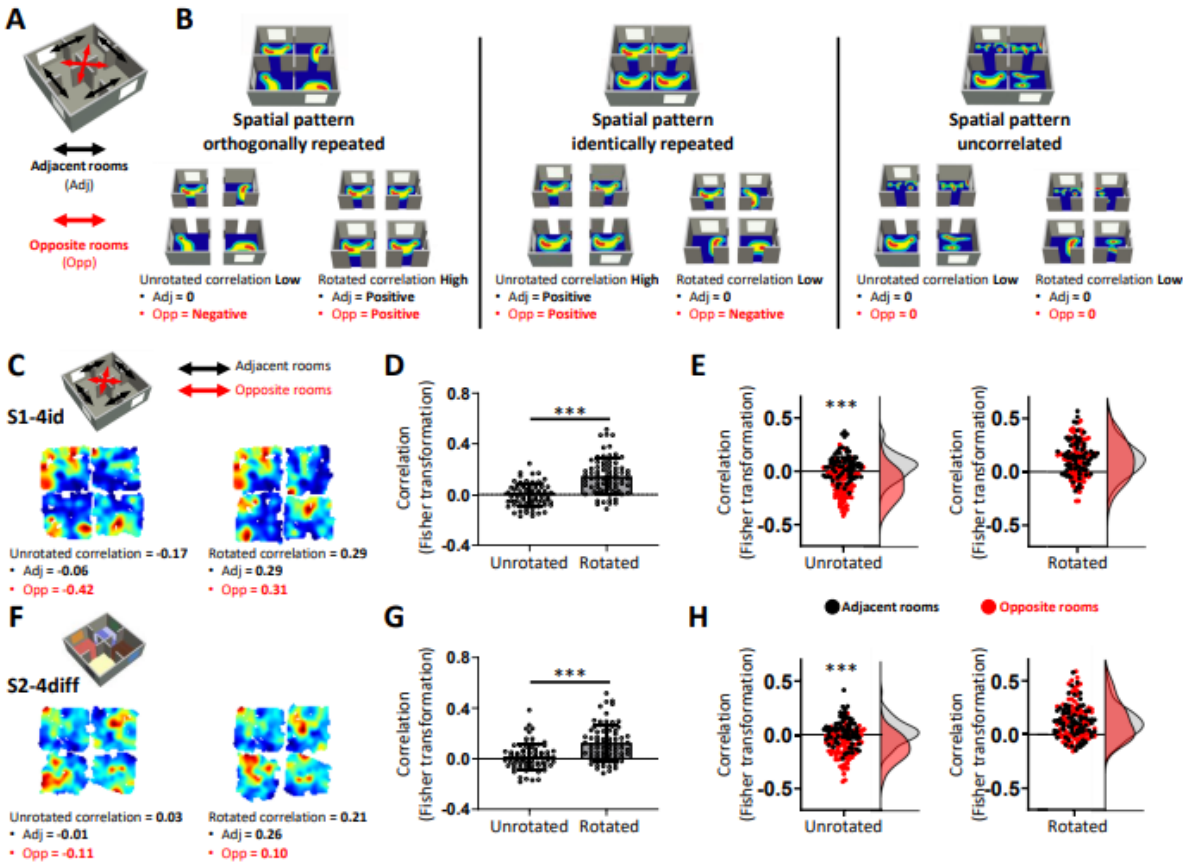


**Figure 5. RSC neuron spatial activity is orthogonally repeated between 4-connected rooms. A.** Diagram of the 4-connected-rooms environment with comparisons between adjacent rooms (black arrows) and opposite rooms (red arrows). **B.** Top: the three hypothetical spatial firing patterns. Bottom: hypothetical spatial correlation for the three patterns, for unrotated and rotated adjacent and opposite rooms. **C-F.** Examples of spatial ratemaps in the 4-identical-connected-rooms (C – S1-4id) and in the 2-different-connected-rooms (F – S2-4diff) environments showing repeating and opposite spatial patterns. **D-G.** The average spatial correlation values reveal that RSC neurons spatial activity correlates better for rotated ratemaps than unrotated ratemaps, for both 4id and 4diff (n = 76). **E-H.** Means and distributions of spatial correlation values for adjacent (black dots) and opposite (red dots) rooms. For unrotated ratemaps, negative correlations are observed between opposite rooms and null correlations between adjacent rooms, while for rotated ratemaps both adjacent and opposite rooms comparisons yield positive correlation values. Individual data are represented by black or red dots. *** $p < 0.001$, Repeated measure ANOVA.

**Hippocampal place cell activity is repeated or remapped but never flipped between rooms.**

The hippocampus connects directly and densely to the granular RSC and indirectly and sparsely to the dysgranular RSC (*Cenquizca & Swanson, 2007; Lomi et al., 2021; Miyashita & Rockland, 2007; Van Groen & Wyss, 1990, 1992, 2003*). The hippocampus possesses place cells whose activity can either remap or be identically repeated in connected rooms environments (*Cheng et al., 2024; Duvelle et al., 2021; Fuhs et al., 2005; Grieves et al., 2016; Paz-Villagrán et al., 2004; Skaggs & McNaughton, 1998; Spiers et al., 2015*). We asked whether the opposite and orthogonal repeated spatial activity found in the RSC can also be observed in hippocampal place cells in the 2- and 4-connected-rooms environments. We recorded neurons from the hippocampus of 4 animals (**Supplementary figure 7**; 3 animals were simultaneously implanted in the RSC) and calculated the spatial correlation between ratemaps of each room that were either unrotated or rotated, to compare with the 3 possible spatial patterns: 1) oppositely and orthogonally repeated in the 2- and the 4-connected-rooms environments respectively; 2) identically repeated; and 3) unrelated between rooms (**Figure 6A and 7A**).

We analyzed 60 place cells in the 2-identical-connected-rooms environment (S1-2id) and followed the activity of 31 of these place cells in the 2-different-connected-rooms environment (S2-2diff) (**Figure 6B-C**). We removed the 5 place cells with place fields located at the door because the analyses will not be able to show a specific spatial activity (**Supplementary figure 8**). We used a value of 0.4 as a threshold to assess significant spatial correlation. We found that place cell activity mainly remaps between rooms in both S1-2id and S2-2diff (51/60 place cells, 85%), a small proportion showing repeated place fields (5/60 place cells, 8%), but no cell displaying opposite or repeated place fields (**Figure 6D-E**). We then tested whether place cell activity was stable between S1-2id and S2-2diff. **Figure 6F** shows that the distribution of the

correlation values between the two environments is bimodal, indicating that place cells activity can be either stable or not (kernel fitting, peaks at 0 and 0.55). We also found that the stability or instability of the firing fields is session dependent (**Supplementary figure 9**), indicating that place cell activity is highly coherent.

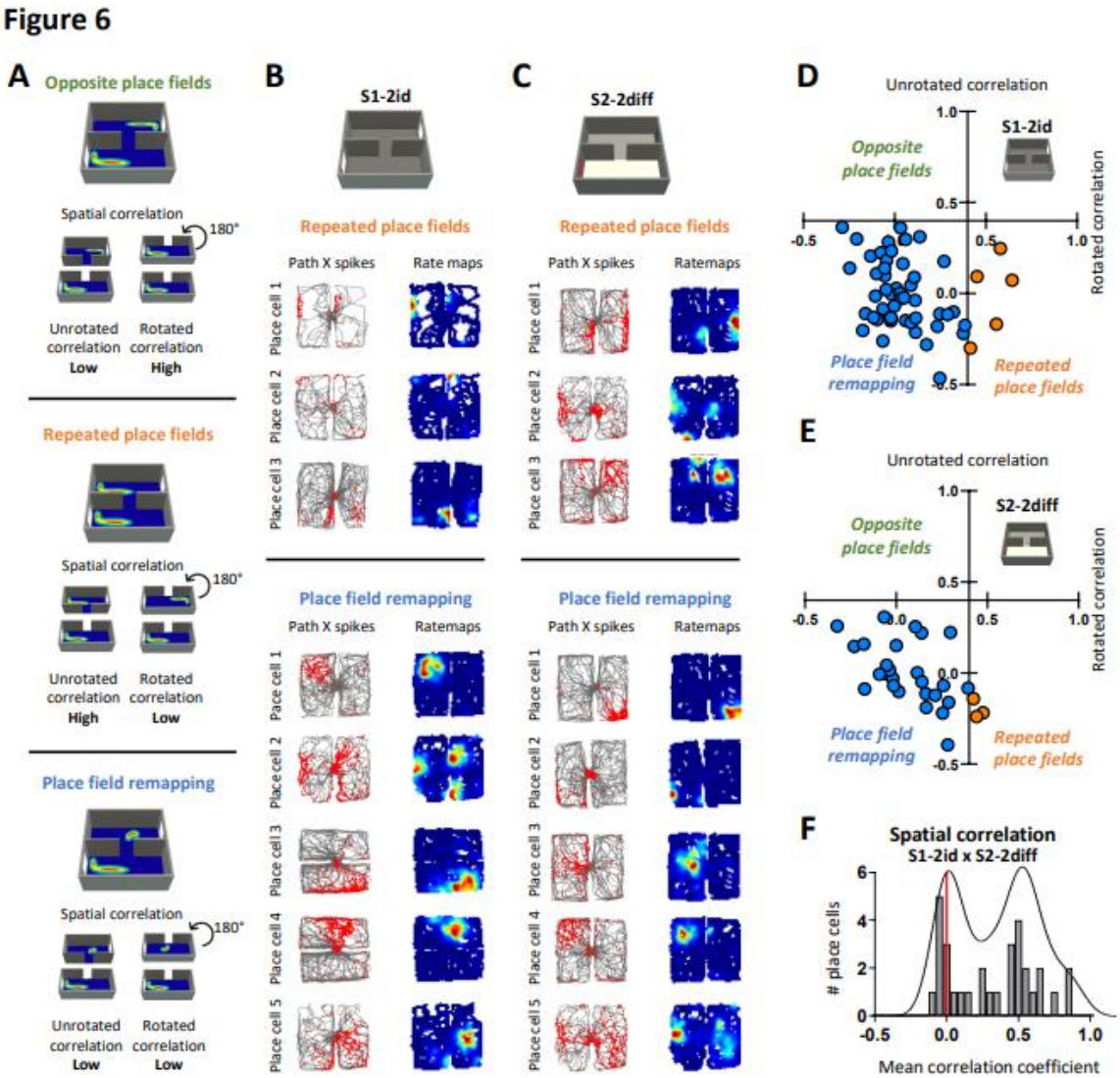


**Figure 6. Hippocampal place cells activity is either repeated or remap between 2-connected-rooms. A.** Three hypothetical spatial patterns observed in the 2-connected-rooms environments (top) and the corresponding correlation (bottom, high *vs* low) between unrotated and rotated ratemaps. **B-C.** Examples of place cells activity with repeating and remapping fields

between rooms for both 2-identical (S1-2id) and 2-different-connected-rooms (S2-2diff) environments. **D-E.** The scatter plot of the correlation values for all place cells according to the three hypothetical spatial patterns (blue: remapping fields, orange: repeated fields, green: opposite fields) reveals that place cells never show opposite place fields for both S1-2id (n = 60) and S2-2diff (n = 31). **F.** Distribution of spatial correlation values of place cell activity between S1-2id and S2-2diff and the corresponding kernel fitting curves, showing stable and unstable place cell activity.

For the 4-connected-rooms environments, we analyzed 206 place cells in 4-identical-connected-rooms (S1-4id) and followed the activity of 141 of these place cells in 4-different-connected-rooms (S2-4diff) (**Figure 7B-C**). We observed that nearly all place cells remap in S1-4id (205/206 place cells, 99.5%), with only one place cell showing a repeated activity (0.5%) (**Figure 7D**). In S2-4diff, we found exclusively place cells that remap between rooms (**Figure 7E**). However, we never observed orthogonally repeated place fields in any of the 4-connected-rooms environment. Finally, we also observed a stable or unstable place cell spatial activity between S1-4id X S2-4diff (kernel fitting, peaks at 0.05 and 0.7), both being session dependent (**Figure 7F**, **Supplementary figure 10**).

## Figure 7

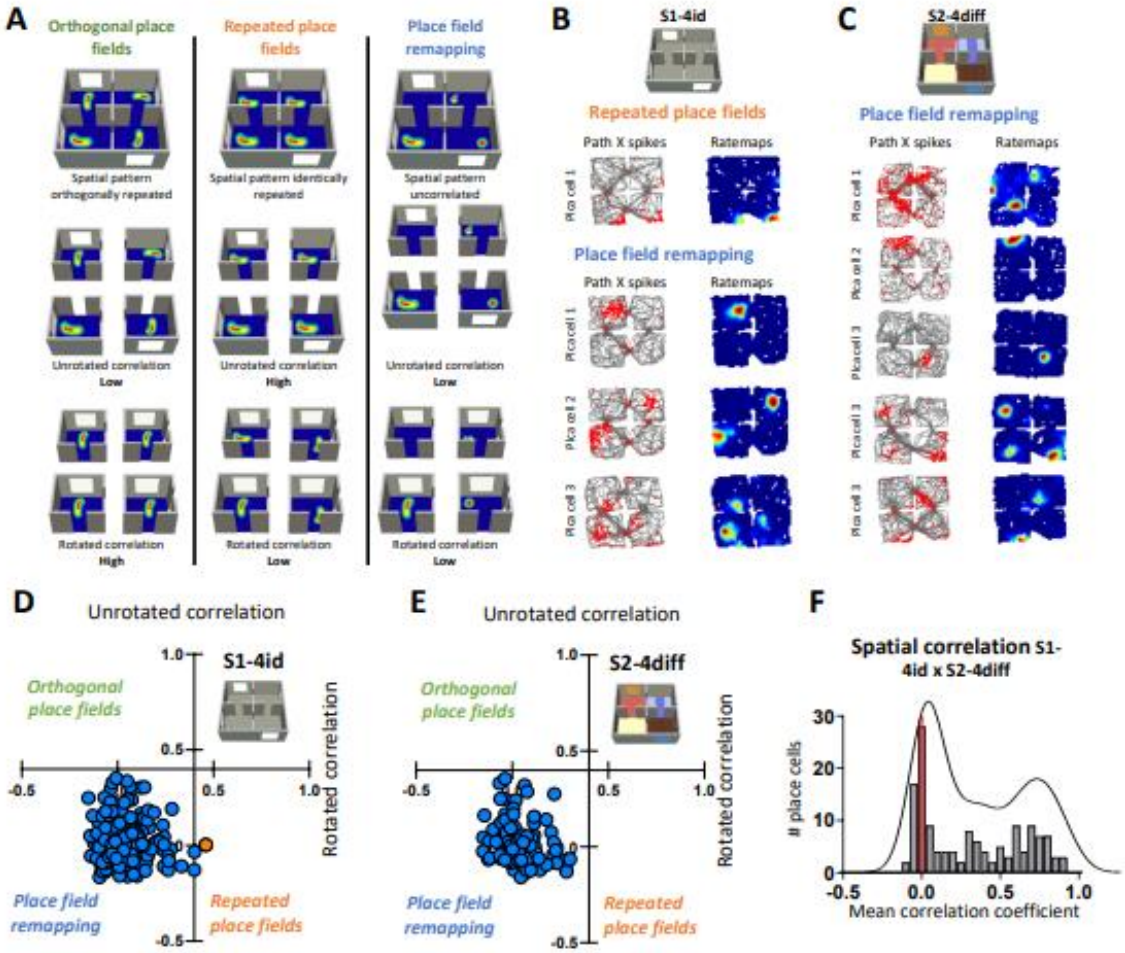


**Figure 7. Hippocampal place cells activity is either repeated or remapped between 4-connected-rooms. A.** Three hypothetical spatial patterns observed in the 4-connected-rooms environment (top), and the corresponding correlation values (bottom, high *vs* low) for unrotated and rotated ratemaps. **B-C.** Examples of place cells with repeating and remapping fields between rooms for both 4-identical (S1-4id) and 4-different (S2-4diff) connected-rooms environments. **D-E.** The scatter plot of correlation values for all place cells according to the three hypothetical spatial patterns (blue: remapping fields, orange: repeated fields, green: orthogonal fields) reveals that place cells show almost exclusively remapping between rooms for both S1-4id (n = 206) and S2-4diff (n = 141). **F.** Distribution of spatial correlation values of place cells activity between S1-4id and S2-4diff and the corresponding kernel fitting curves, showing stable and unstable place cell activity.

# Discussion

Since its discovery, the HD system is thought to orient animals' navigation regardless of the complexity of the environment (*Chen et al., 1994; Cho & Sharp, 2001; Dudchenko & Zinyuk, 2005; Taube et al., 1990; Taube & Burton, 1995; Yoder et al., 2011*). Here we show that alongside the HDCs that maintain the same PFD between connected spaces, the RSC contains another population of directionally modulated cells, the MDCs, having PFD that change between connected rooms. Previous studies describing MDCs activity have used rooms that are visually and tactilely identical (*Jacob et al., 2017; Zhang et al., 2022*) possibly making rooms difficult to tell apart for the rats, thus questioning the nature of the multidirectional pattern that could arise from the repetition of similar external cues. We invalidated this visual ambiguity effect by showing that MDCs activity is present when the rooms are different. In addition, we recorded BDCs where there were no odors to distinguish between rooms (unlike in previous studies), suggesting that visual and tactile information are sufficient to support the firing of BDCs and HDCs. We also observed that MDCs show opposite bidirectional activity in an environment composed of two opposite rooms, and orthogonal directional activity in four rooms arranged orthogonally. This indicates that increasing the number of connected rooms (from two to four) leads to an increase in the number of directional activities that are anchored to the relative orientation of the rooms. Analyses of cells' activity specific to the rooms revealed that MDCs have unipolar activity within each room, resembling an HDC. When following cells activity between the 2-rooms and 4-rooms environments, the MDCs maintained their multidirectional activity while the HDCs always remain unipolar and therefore never become multidirectional. This strongly suggests that MDCs and HDCs form two distinct populations of directional cells, thus challenging the hypothesis of a single HD system in which all HDCs are integrated into a unique attractor network (*Clarck & Taube, 2012; Redish et al., 1996; Skaggs*

*et al., 1995; Zhang, 1996*). Thus, several HDCs attractor networks possibly exist in the brain (*Kornienko et al., 2018; LaChance et al., 2022; Samsonovich, 2018*), or not all RSC directional cells belong to the unique attractor network and their activity may not be explained by attractor dynamics (*Page & Jeffery, 2018; Yan et al., 2021*). Future studies will help sort out these alternative hypotheses.

A crucial question is to identify what determines the multidirectional pattern of MDCs? A possibility is that a single feature of the environment shapes this firing pattern, such as the door. However, in the 4-rooms environments, the animal can access rooms through 2 doors, each leading to an adjacent room, but we never observed MDCs with orthogonal bidirectional activity in a single room. Similarly, Zhang *et al.* study (2022) showed that MDCs have unipolar activity in single compartments while animals entered to the rooms via a unique central door. This suggests that the number of doors does not determine the multidirectional firing. Moreover, it is unlikely that visual cues shape MDCs firing, since the multidirectional activity is maintained in total darkness (*Jacob et al., 2017; Zhang et al., 2022*). Finally, it is unconvincing that MDCs are egocentric boundary vector cells as their PFDs are uniformly distributed in all directions and not clustered according to the orientation of the walls, as well as MDCs fire at every position and not just close to the walls (*Alexander et al., 2020*). Therefore, we propose that the key factor is not a single feature of the environment, but rather the ensemble of elements (environmental features, symmetry and orientation of the rooms, topology, navigation, goals, etc.) that make it possible to determine what constitutes the local and global reference frames. In return, these frames are essential for navigating in connected rooms.

A room limited by walls provides a single reference frame which includes both spatial and non-spatial features. In a more complex environment made of several connected rooms, there will be as many local reference frames as there will be rooms visited by the subject. A global

reference frame unifies the set of local rooms into an overall representation and gives access to the spatial organization of the environment in its totality as well as to the way by which the local rooms are connected with each other (the topology). Thus, the subject can infer the most direct and efficient path between two distant places and navigate efficiently between rooms. MDCs activities are consistent with a role of the RSC in anchoring the spatial map within local reference frames, since their PFDs change each time the animal moves from one room to another. In contrast, HDCs that maintain the same PFD can anchor the spatial map in a global reference frame in multicompartment environments. Single room space as an open field is a special case in which either the unique local reference frame merges with the global one, or there is no local reference frame but only a global one. It is therefore not surprising to observe that the activity of MDCs is lost or becomes unidirectional while HDCs activity remains unchanged (*Jacob et al., 2017; Zhang et al., 2022*).

MDCs and HDCs account for around 10% of neurons in the RSC, which also contain cells with either other spatial correlates such as position and movement (*Alexander et al., 2015, 2017, 2020; Chen et al., 1994; Cho & Sharp, 2001; Keshavarzi et al., 2021; Mao et al., 2018; Miller et al., 2019, 2021; Smith et al., 2012*) or no directly observable spatial correlates (*Auger & Maguire, 2018; Todd et al., 2019*). We analyzed non-directional cells and found that they carry spatial information that is anchored to the features of the room, *i.e.* showing repeated opposite activity in the 2-connected-rooms environments and repeated orthogonal activity in the 4-connected-rooms environments. Interestingly, we found that hippocampal place cell activity could be either different or identical between rooms, but never oppositely or orthogonally repeated as observed in the RSC, indicating that the two structures do not represent the local space in the same way. Moreover, place cells activity showed either remapping or repetition of place fields between rooms, but never the two simultaneously (*Grieves et al., 2016, 2017;*

*Harland et al., 2017; Paz-Villagran et al., 2004; Spiers et al., 2015*). Similarly, the entorhinal cortex, which is directly connected to the RSC (*Burwell & Amaral, 1998; Czajkowski et al., 2013; Jones & Witter, 2007; Shibata, 1994; Sugar & Witter, 2016; Van Groen & Wyss, 1992*), contains grid cells that code for animal position and are anchored to either local or global spaces but not both simultaneously (*Carpenter et al., 2015; Derdikman et al., 2009; Sanguinetti-Scheck & Brecht, 2020*). In contrast, MDCs and HDCs were observed simultaneously in the RSC. These findings highlight the RSC as the unique and critical brain structure to form spatial representations within different reference frames simultaneously. These local *vs* global representations could be conveyed to the hippocampal and entorhinal spatial systems which use one of the two reference frames, possibly depending on the information that is appropriate for the animal current behavior or current environment.

Along with findings of simultaneous coding of both allocentric and egocentric space in the RSC in humans and rodents (*Alexander et al., 2015, 2020, 2023; Byrne et al., 2007; Clark et al., 2018; Kim & Maguire, 2018; Marchette et al., 2014; Peer et al., 2019; Shine et al., 2016; Van Wijngaarden et al., 2020; Vann et al., 2009*), our findings suggest that the RSC system establishes a representation of space by combining different spatial dimensions. The integration of all these dimensions in a coherent representation within the retrosplenial-entorhinal-hippocampal network may support the ability to navigate in complex spaces.

# Acknowledgments

This work was supported by a grant from the Agence Nationale de la Recherche (ANR-21-CE37-0006-01), by the Centre National de la Recherche Scientifique (CNRS) and Aix-Marseille University (AMU). We thank the Spatial Cognition group for their insightful

comments on the manuscript, S. Quitard for the histological work, the Olympique de Marseille and Jul. C. Laurent salary for this work was provided by the ANR grant.

## Author contributions

C.L., P.Y.J. and F.S. designed the study. C.L. and P.Y.J. performed surgeries and recordings. C.L. & P.Y.J. analyzed data. All authors interpreted data and discussed results. C.L. and P.Y.J. wrote the manuscript. All authors commented and edited the manuscript.

## Competing interests

The authors declare no competing financial interests.

## References

1. Alexander, A. S., Carstensen, L. C., Hinman, J. R., Raudies, F., Chapman, G. W. & Hasselmo, M. E. Egocentric boundary vector tuning of the retrosplenial cortex. *SCIENCE ADVANCES* (2020).

2. Alexander, A. S. & Nitz, D. A. Retrosplenial cortex maps the conjunction of internal and external spaces. *Nat Neurosci* **18**, 1143–1151 (2015).

3. Alexander, A. S. & Nitz, D. A. Spatially Periodic Activation Patterns of Retrosplenial Cortex Encode Route Sub-spaces and Distance Traveled. *Current Biology* **27**, 1551-1560.e4 (2017).

4. Alexander, A. S., Robinson, J. C., Stern, C. E. & Hasselmo, M. E. Gated transformations from egocentric to allocentric reference frames involving retrosplenial cortex, entorhinal cortex, and hippocampus. *Hippocampus* **33**, 465–487 (2023).

5. Auger, S. D. & Maguire, E. A. Retrosplenial Cortex Indexes Stability beyond the Spatial Domain. *J. Neurosci.* **38**, 1472–1481 (2018).

6. Burwell, R. D. & Amaral, D. G. Cortical afferents of the perirhinal, postrhinal, and entorhinal cortices of the rat. *J. Comp. Neurol.* **398**, 179–205 (1998).

7. Byrne, P., Becker, S. & Burgess, N. Remembering the past and imagining the future: A neural model of spatial memory and imagery. *Psychological Review* **114**, 340–375 (2007).

8. Carpenter, F., Manson, D., Jeffery, K., Burgess, N. & Barry, C. Grid Cells Form a Global Representation of Connected Environments. *Current Biology* **25**, 1176–1182 (2015).

9. Cenquizca, L. A. & Swanson, L. W. Spatial organization of direct hippocampal field CA1 axonal projections to the rest of the cerebral cortex. *Brain Research Reviews* **56**, 1–26 (2007).

10. Chen, L. L., Lin, L.-H. & Green, E. J. Head-direction cells in the rat posterior cortex. (1994).

11. Cheng, H. Y., Overington, D. W. & Jeffery, K. J. A configural context signal simultaneously but separably drives positioning and orientation of hippocampal place fields. *Hippocampus* **34**, 73–87 (2024).

12. Cho & Sharp. Head direction, place, and movement correlates for cells in the rat retrosplenial cortex. (2001).

13. Clark, B. J., Simmons, C. M., Berkowitz, L. E. & Wilber, A. A. The retrosplenial-parietal network and reference frame coordination for spatial navigation. *Behavioral Neuroscience* **132**, 416–429 (2018).

14. Clark, B. J. & Taube, J. S. Vestibular and attractor network basis of the head direction cell signal in subcortical circuits. *Front. Neural Circuits* **6**, (2012).

15. Czajkowski, R., Sugar, J., Zhang, S.-J., Couey, J. J., Ye, J. & Witter, M. P. Superficially Projecting Principal Neurons in Layer V of Medial Entorhinal Cortex in the Rat Receive Excitatory Retrosplenial Input. *J. Neurosci.* **33**, 15779–15792 (2013).

16. Derdikman, D., Whitlock, J. R., Tsao, A., Fyhn, M., Hafting, T., Moser, M.-B. & Moser, E. I. Fragmentation of grid cell maps in a multicompartment environment. *Nat Neurosci* **12**, 1325–1332 (2009).

17. Dudchenko, P. A. & Zinyuk, L. E. The formation of cognitive maps of adjacent environments: Evidence from the head direction cell system. *Behavioral Neuroscience* **119**, 1511–1523 (2005).

18. Duvelle, É., Grieves, R. M., Liu, A., Jedidi-Ayoub, S., Holeniewska, J., Harris, A., Nyberg, N., Donnarumma, F., Lefort, J. M., Jeffery, K. J., Summerfield, C., Pezzulo, G. & Spiers, H. J. Hippocampal place cells encode global location but not connectivity in a complex space. *Current Biology* **31**, 1221-1233.e9 (2021).

19. Fuhs, M. C., VanRhoads, S. R., Casale, A. E., McNaughton, B. & Touretzky, D. S. Influence of Path Integration Versus Environmental Orientation on Place Cell Remapping Between Visually Identical Environments. *Journal of Neurophysiology* **94**, 2603–2616 (2005).

20. Grieves, R. M., Duvelle, É., Wood, E. R. & Dudchenko, P. A. Field repetition and local mapping in the hippocampus and the medial entorhinal cortex. *Journal of Neurophysiology* **118**, 2378–2388 (2017).

21. Grieves, R. M., Jenkins, B. W., Harland, B. C., Wood, E. R. & Dudchenko, P. A. Place field repetition and spatial learning in a multicompartment environment. *Hippocampus* **26**, 118–134 (2016).

22. Harland, B., Grieves, R. M., Bett, D., Stentiford, R., Wood, E. R. & Dudchenko, P. A. Lesions of the Head Direction Cell System Increase Hippocampal Place Field Repetition. *Current Biology* **27**, 2706-2712.e2 (2017).

23. Insausti, R., Herrero, M. T. & Witter, M. P. Entorhinal cortex of the rat: Cytoarchitectonic subdivisions and the origin and distribution of cortical efferents. *Hippocampus* **7**, 146–183 (1997).

24. Jacob, P.-Y., Casali, G., Spieser, L., Page, H., Overington, D. & Jeffery, K. An independent, landmark-dominated head-direction signal in dysgranular retrosplenial cortex. *Nat Neurosci* **20**, 173–175 (2017).

25. Jones, B. F. & Witter, M. P. Cingulate cortex projections to the parahippocampal region and hippocampal formation in the rat. *Hippocampus* **17**, 957–976 (2007).

26. Keshavarzi, S., Bracey, E. F., Faville, R. A., Campagner, D., Tyson, A. L., Lenzi, S. C., Branco, T. & Margrie, T. W. The retrosplenial cortex combines internal and external cues to encode head velocity during navigation. Preprint at https://doi.org/10.1101/2021.01.22.427789 (2021).

27. Kim, M. & Maguire, E. A. Hippocampus, Retrosplenial and Parahippocampal Cortices Encode Multicompartment 3D Space in a Hierarchical Manner. *Cerebral Cortex* **28**, 1898–1909 (2018).

28. Kornienko, O., Latuske, P., Bassler, M., Kohler, L. & Allen, K. Non-rhythmic head-direction cells in the parahippocampal region are not constrained by attractor network dynamics. *eLife* **7**, e35949 (2018).

29. LaChance, P. A., Graham, J., Shapiro, B. L., Morris, A. J. & Taube, J. S. Landmark-modulated directional coding in postrhinal cortex. *Sci. Adv.* **8**, eabg8404 (2022).

30. Lomi, E., Mathiasen, M. L., Cheng, H. Y., Zhang, N., Aggleton, J. P., Mitchell, A. S. & Jeffery, K. J. Evidence for two distinct thalamocortical circuits in retrosplenial cortex. *Neurobiology of Learning and Memory* **185**, 107525 (2021).

31. Lozano, Y. R., Page, H., Jacob, P.-Y., Lomi, E., Street, J. & Jeffery, K. Retrosplenial and postsubicular head direction cells compared during visual landmark discrimination. *Brain and Neuroscience Advances* **1**, 239821281772185 (2017).

32. Mao, D., Kandler, S., McNaughton, B. L. & Bonin, V. Sparse orthogonal population representation of spatial context in the retrosplenial cortex. *Nat Commun* **8**, 243 (2017).

33. Mao, D., Neumann, A. R., Sun, J., Bonin, V., Mohajerani, M. H. & McNaughton, B. L. Hippocampus-dependent emergence of spatial sequence coding in retrosplenial cortex. *Proc. Natl. Acad. Sci. U.S.A.* **115**, 8015–8018 (2018).

34. Marchette, S. A., Vass, L. K., Ryan, J. & Epstein, R. A. Anchoring the neural compass: coding of local spatial reference frames in human medial parietal lobe. *Nat Neurosci* **17**, 1598–1606 (2014).

35. Milczarek, M. M., Vann, S. D. & Sengpiel, F. Spatial Memory Engram in the Mouse Retrosplenial Cortex. *Current Biology* **28**, 1975-1980.e6 (2018).

36. Miller, A. M. P., Serrichio, A. C. & Smith, D. M. Dual-Factor Representation of the Environmental Context in the Retrosplenial Cortex. *Cerebral Cortex* **31**, 2720–2728 (2021).

37. Miller, A. M. P., Mau, W. & Smith, D. M. Retrosplenial Cortical Representations of Space and Future Goal Locations Develop with Learning. *Current Biology* **29**, 2083-2090.e4 (2019).

38. Mitchell, A. S., Czajkowski, R., Zhang, N., Jeffery, K. & Nelson, A. J. D. Retrosplenial cortex and its role in spatial cognition. *Brain and Neuroscience Advances* **2**, 239821281875709 (2018).

39. Miyashita, T. & Rockland, K. S. GABAergic projections from the hippocampus to the retrosplenial cortex in the rat. *Eur J of Neuroscience* **26**, 1193–1204 (2007).

40. Muller, R., Kubie, J. & Ranck, J. Spatial firing patterns of hippocampal complex-spike cells in a fixed environment. *J. Neurosci.* **7**, 1935–1950 (1987).

41. Naber, P. A., Lopes Da Silva, F. H. & Witter, M. P. Reciprocal connections between the entorhinal cortex and hippocampal fields CA1 and the subiculum are in register with the projections from CA1 to the subiculum. *Hippocampus* **11**, 99–104 (2001).

42. Page, H. J. I. & Jeffery, K. J. Landmark-Based Updating of the Head Direction System by Retrosplenial Cortex: A Computational Model. *Front. Cell. Neurosci.* **12**, 191 (2018).

43. Paxinos, G. & Watson, C. *The Rat Brain in Stereotaxic Coordinates*. (Academic Press, 6th edn., 2007).

44. Paz-Villagrán, V., Save, E. & Poucet, B. Independent coding of connected environments by place cells. *Eur J of Neuroscience* **20**, 1379–1390 (2004).

45. Peer, M., Ron, Y., Monsa, R. & Arzy, S. Processing of different spatial scales in the human brain. *eLife* **8**, e47492 (2019).

46. Redish, A. D., Elga, A. N. & Touretzky, D. S. A coupled attractor model of the rodent head direction system. (1996).

47. Samsonovich, A. V. A Continuous-Attractor Model of Flip Cell Phenomena. in *Biologically Inspired Cognitive Architectures (BICA) for Young Scientists* (eds. Samsonovich, A. V. & Klimov, V. V.) vol. 636 163–172 (Springer International Publishing, Cham, 2018).

48. Sanguinetti-Scheck, J. I. & Brecht, M. Home, head direction stability, and grid cell distortion. *Journal of Neurophysiology* **123**, 1392–1406 (2020).

49. Sherrill, K. R., Erdem, U. M., Ross, R. S., Brown, T. I., Hasselmo, M. E. & Stern, C. E. Hippocampus and Retrosplenial Cortex Combine Path Integration Signals for Successful Navigation. *J. Neurosci.* **33**, 19304–19313 (2013).

50. Shibata, H. Terminal distribution of projections from the retrosplenial area to the retrohippocampal region in the rat, as studied by anterograde transport of biotinylated dextran amine. *Neuroscience Research* **20**, 331–336 (1994).

51. Shine, J. P., Valdés-Herrera, J. P., Hegarty, M. & Wolbers, T. The Human Retrosplenial Cortex and Thalamus Code Head Direction in a Global Reference Frame. *J. Neurosci.* **36**, 6371–6381 (2016).

52. Skaggs, W. E., Knierim, J. J., Kudrimoti, H. S. & McNaughton, B. L. A Model of the Neural Basis of the Rat's Sense of Direction. (1995).

53. Skaggs, W. E. & McNaughton, B. L. Spatial Firing Properties of Hippocampal CA1 Populations in an Environment Containing Two Visually Identical Regions. *J. Neurosci.* **18**, 8455–8466 (1998).

54. Smith, D. M., Barredo, J. & Mizumori, S. J. Y. Complimentary roles of the hippocampus and retrosplenial cortex in behavioral context discrimination. *Hippocampus* **22**, 1121–1133 (2012).

55. Spiers, H. J., Hayman, R. M. A., Jovalekic, A., Marozzi, E. & Jeffery, K. J. Place Field Repetition and Purely Local Remapping in a Multicompartment Environment. *Cerebral Cortex* **25**, 10–25 (2015).

56. Subramanian, D. L., Miller, A. M. P. & Smith, D. M. A comparison of hippocampal and retrosplenial cortical spatial and contextual firing patterns. *Hippocampus* **34**, 357–377 (2024).

57. Sugar, J. & Witter, M. P. Postnatal development of retrosplenial projections to the parahippocampal region of the rat. *eLife* **5**, e13925 (2016).

58. Sulpizio, V., Committeri, G., Lambrey, S., Berthoz, A. & Galati, G. Selective role of lingual/parahippocampal gyrus and retrosplenial complex in spatial memory across viewpoint changes relative to the environmental reference frame. *Behavioural Brain Research* **242**, 62–75 (2013).

59. Takahashi, N., Kawamura, M., Shiota, J., Kasahata, N. & Hirayama, K. Pure topographic disorientation due to right retrosplenial lesion. *Neurology* **49**, 464–469 (1997).

60. Taube, J. S. & Burton, H. L. Head direction cell activity monitored in a novel environment and during a cue conflict situation. *Journal of Neurophysiology* **74**, 1953–1971 (1995).

61. Taube, J., Muller, R. & Ranck, J. Head-direction cells recorded from the postsubiculum in freely moving rats. I. Description and quantitative analysis. *J. Neurosci.* **10**, 420–435 (1990).

62. Todd, T. P., Fournier, D. I. & Bucci, D. J. Retrosplenial cortex and its role in cue-specific learning and memory. *Neurosci Biobehav Rev* **107**, 713–728 (2019).

63. Van Groen, T. & Michael Wyss, J. Connections of the retrosplenial granular a cortex in the rat. *J of Comparative Neurology* **300**, 593–606 (1990).

64. Van Groen, T. & Wyss, J. M. Connections of the retrosplenial granular b cortex in the rat. *J of Comparative Neurology* **463**, 249–263 (2003).

65. Van Wijngaarden, J. B., Babl, S. S. & Ito, H. T. Entorhinal-retrosplenial circuits for allocentric-egocentric transformation of boundary coding. *eLife* **9**, e59816 (2020).

66. Vann, S. D., Aggleton, J. P. & Maguire, E. A. What does the retrosplenial cortex do? *Nat Rev Neurosci* **10**, 792–802 (2009).

67. Vedder, L. C., Miller, A. M. P., Harrison, M. B. & Smith, D. M. Retrosplenial Cortical Neurons Encode Navigational Cues, Trajectories and Reward Locations During Goal Directed Navigation. *Cereb. Cortex* cercor;bhw192v1 (2016).

68. Vélez-Fort, M., Bracey, E. F., Keshavarzi, S., Rousseau, C. V., Cossell, L., Lenzi, S. C., Strom, M. & Margrie, T. W. A Circuit for Integration of Head- and Visual-Motion Signals in Layer 6 of Mouse Primary Visual Cortex. *Neuron* **98**, 179-191.e6 (2018).

69. Vogt, B. A. & Miller, M. W. Cortical connections between rat cingulate cortex and visual, motor, and postsubicular cortices. *J of Comparative Neurology* **216**, 192–210 (1983).

70. Wyss, J. M. & Van Groen, T. Connections between the retrosplenial cortex and the hippocampal formation in the rat: A review. *Hippocampus* **2**, 1–11 (1992).

71. Xie, H., Liu, Y., Zhu, Y., Ding, X., Yang, Y. & Guan, J.-S. In vivo imaging of immediate early gene expression reveals layer-specific memory traces in the mammalian brain. *Proc. Natl. Acad. Sci. U.S.A.* **111**, 2788–2793 (2014).

72. Yan, Y., Burgess, N. & Bicanski, A. A model of head direction and landmark coding in complex environments. *PLoS Comput Biol* **17**, e1009434 (2021).

73. Yoder, R. M., Clark, B. J., Brown, J. E., Lamia, M. V., Valerio, S., Shinder, M. E. & Taube, J. S. Both visual and idiothetic cues contribute to head direction cell stability during navigation along complex routes. *Journal of Neurophysiology* **105**, 2989–3001 (2011).

74. Zhang, K. Representation of spatial orientation by the intrinsic dynamics of the head-direction cell ensemble: a theory. *J. Neurosci.* **16**, 2112–2126 (1996).

75. Zhang, N., Grieves, R. M. & Jeffery, K. J. Environment Symmetry Drives a Multidirectional Code in Rat Retrosplenial Cortex. *J. Neurosci.* **42**, 9227–9241 (2022).

# Supplementary figures

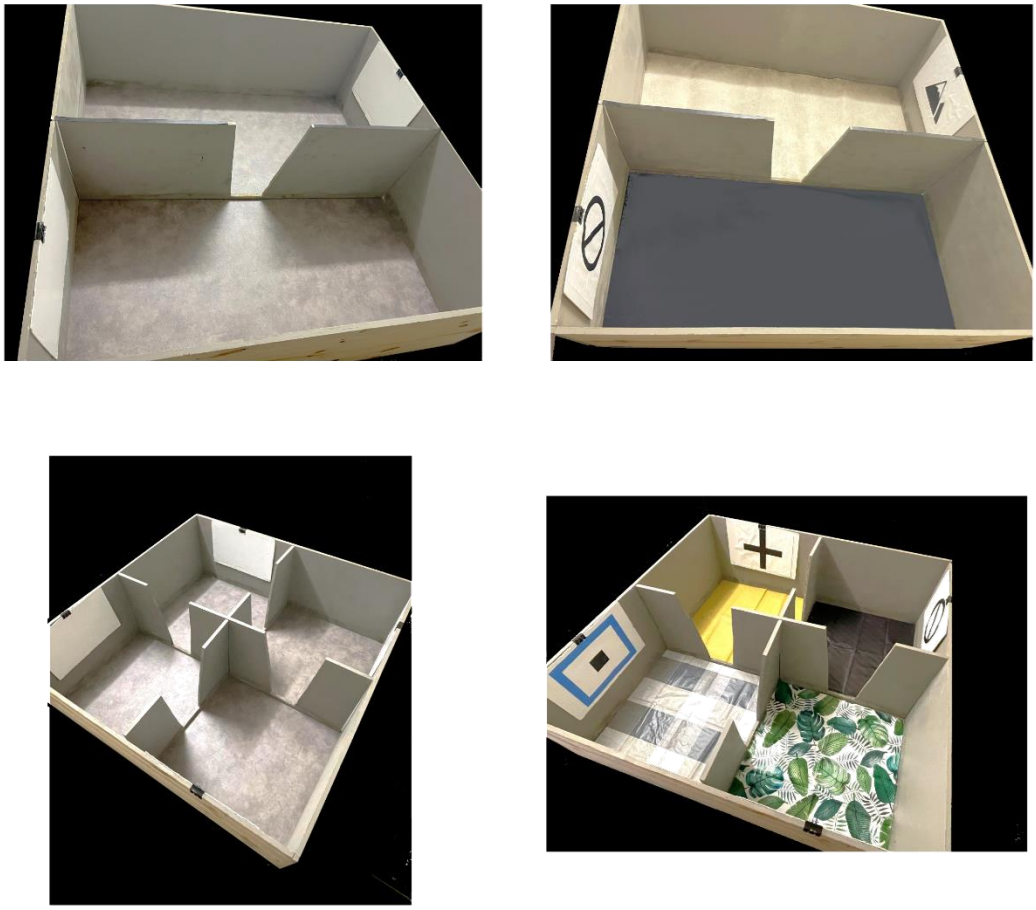

**Supplementary figure 1 – Pictures of the 4 connected rooms environment.**
**A.** The 2 identical connected rooms environment (same visual cues and floor). B. The 2 different connected rooms environment (different visual cues and floor colors and textures). C. The 4 identical connected rooms environment (same visual cues and floor). D. The 4 different connected rooms environment (different visual cues and floor colors and textures).

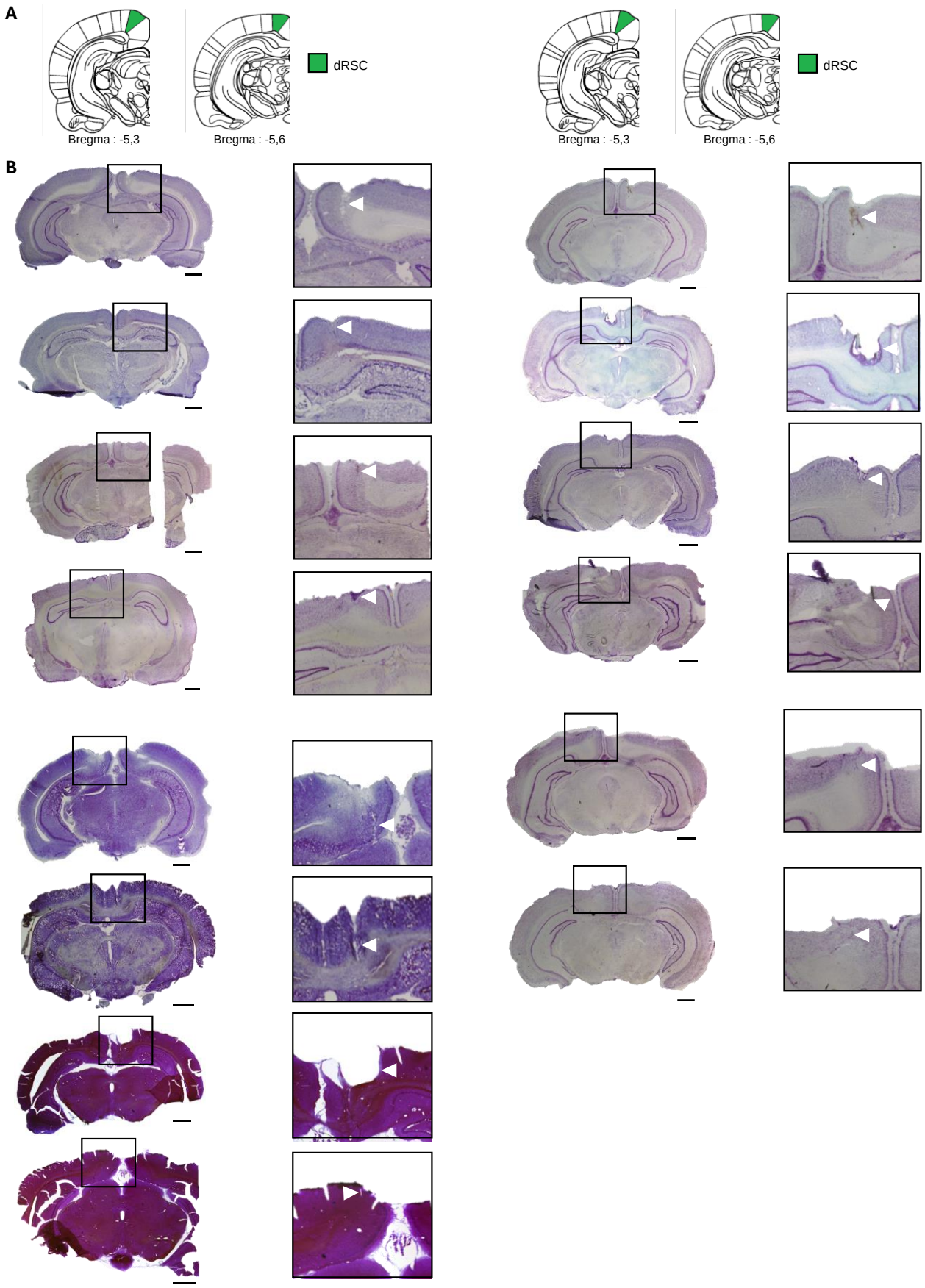
A
Bregma : -5,3
Bregma : -5,6
dRSC
Bregma : -5,3
Bregma : -5,6
dRSC
B

**Supplementary figure 2 – Histology retrosplenial cortex.**

**A.** Diagram showing the location of the dysgranular retrosplenial animals (RSC) adapted from Paxinos G, Watson C. The Rat Brain in Stereotaxic Coordinates. 4th Edition. Academic Press 1998.

**B.** Coronal slices through the region of electrode implantation from the RSC (black insets) with scale bars indicating 1 mm. Bottom right: magnification of insets to visualize the track of electrodes (white arrow).

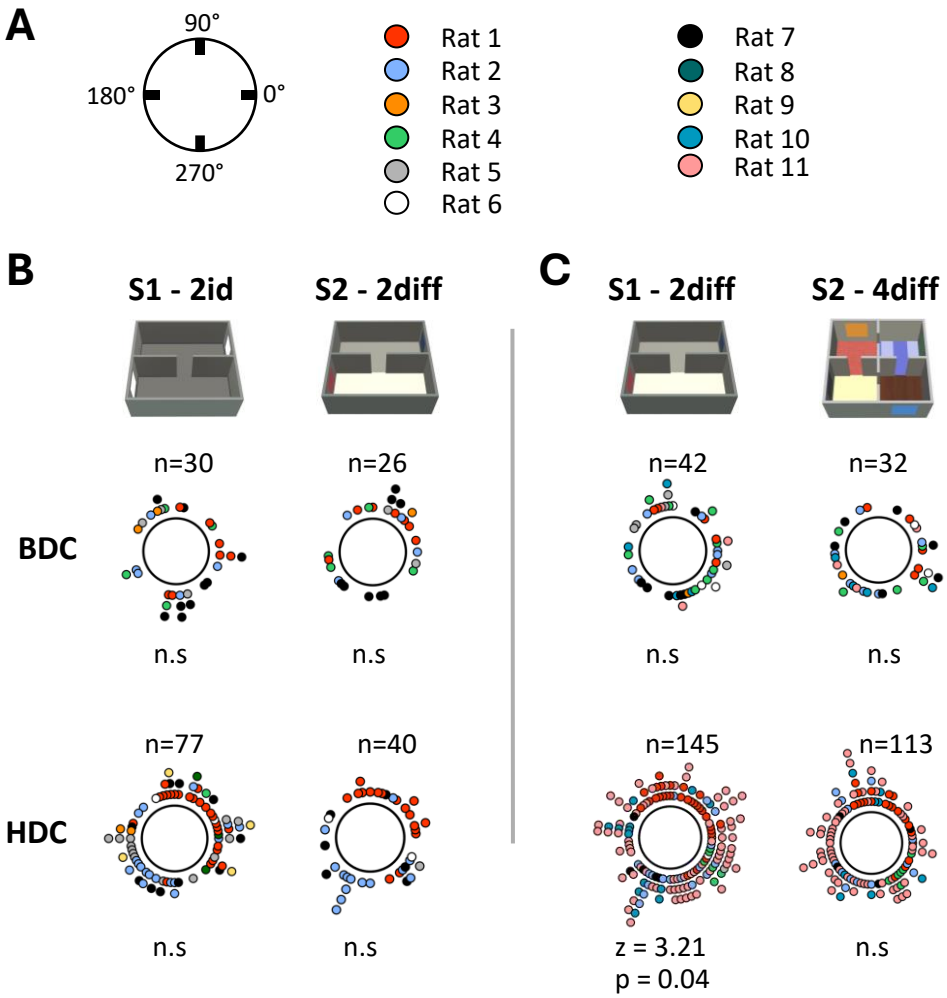


**Supplementary figure 3 – Directional firing of RSC BDC and HDC**
**A.** Left: Diagram of firing direction, Right: color code for each rat.
**B.** Polar distribution of PFD for both BDCs (middle) and HDCs (bottom) was homogeneous (determined by Rayleigh test) for the 2 connected room environments.
**C.** Polar distribution of PFD for BDCs (middle) was homogeneous (determined by Rayleigh test) for both the 2 and 4 connected room environments (middle) and for HDCs for the 4 connected rooms environment (bottom right), while the distribution of PFD was clustered for HDCs in the 2 different connected rooms environment (bottom left).

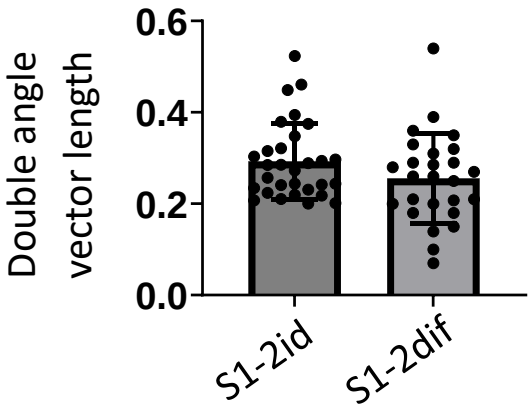


**Supplementary figure 4 – Comparison of directional activity for BDCs in 2 connected rooms environments.**

Means of Rayleigh vector length after using the double-angle procedure for BDCs directional firing (see Meethods) show no difference between 2 identical and 2 difference connected rooms environments.

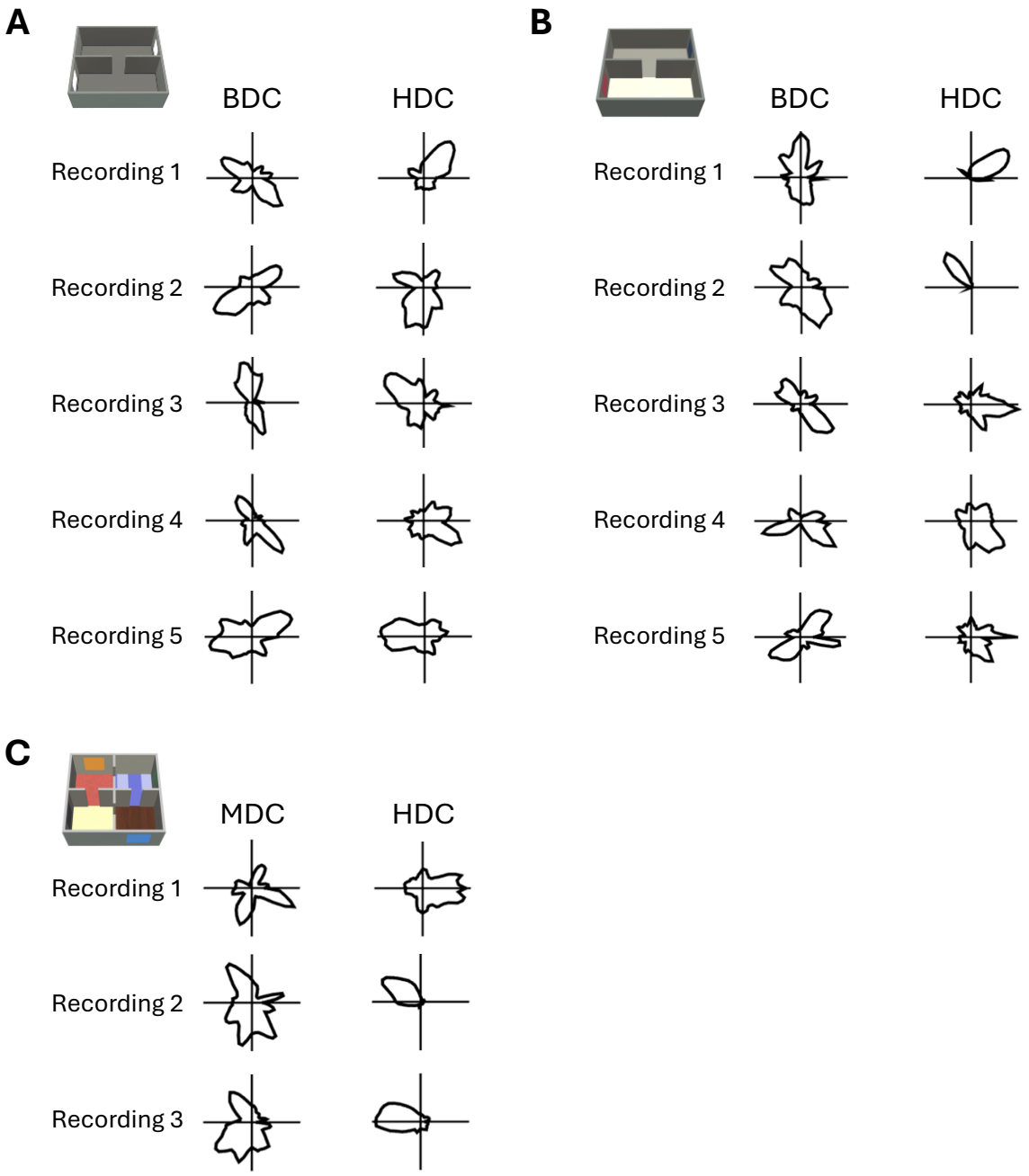


**Supplementary figure 5 – Simultaneous recording of BDCs / MDCs and HDCs.**
**A.** 5 examples from 5 different days and 4 different animals of simultaneous recordings of BDCs and HDCs in the 2 identical connected rooms environment.
**B.** 5 examples from 5 different days and 3 different animals of simultaneous recordings of BDCs and HDCs in the 2 different connected rooms environment.
**C.** 3 examples from 2 different days and 2 different animals of simultaneous recordings of MDCs and HDCs in the 4 different connected rooms environment.

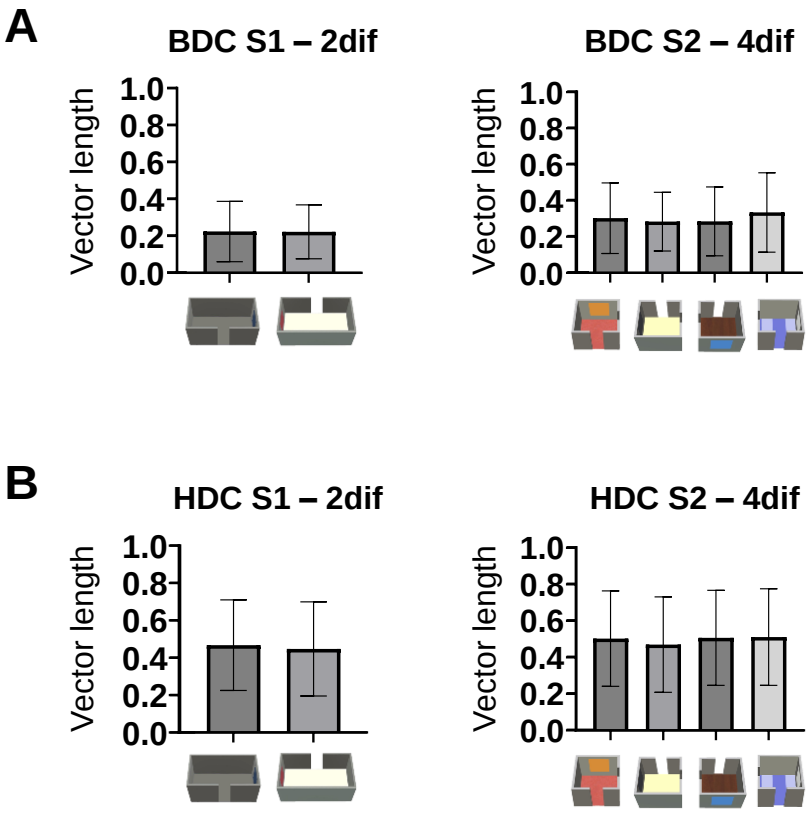


**Supplementary figure 6 – Comparison of Rayleigh vector length between rooms.**
Means of Rayleigh vector length for each room in isolation show no difference for both BDCs (**A**) and HDCs (**B**) whether the rooms were identical (left) or different (right).

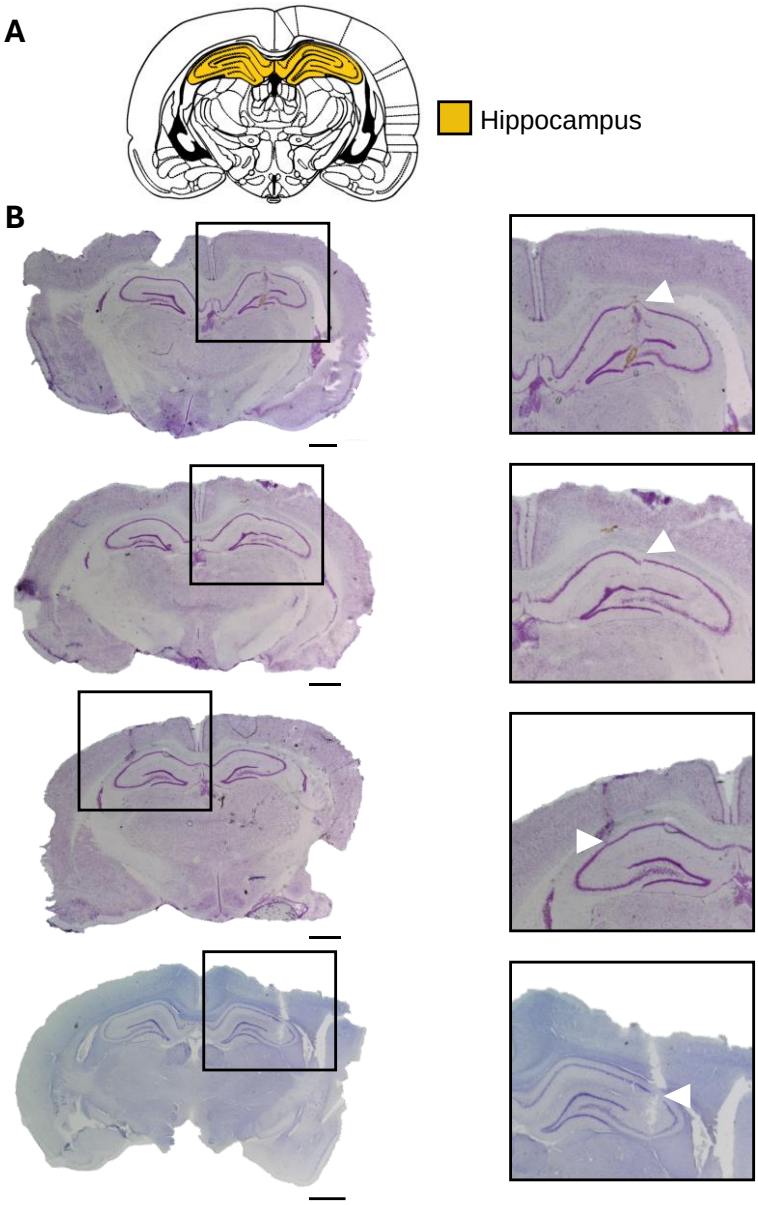


**Supplementary figure 7 – Histology hippocampus.**
**A.** Diagram showing the location of the hippocampus (HPC) adapted from Paxinos G, Watson C. The Rat Brain in Stereotaxic Coordinates. 4th Edition. Academic Press 1998.
**B.** Coronal slices through the region of electrode implantation from the HPC (black insets) with scale bars indicating 1 mm. Bottom right: Magnification of insets to visualize the track of electrodes (white arrow).

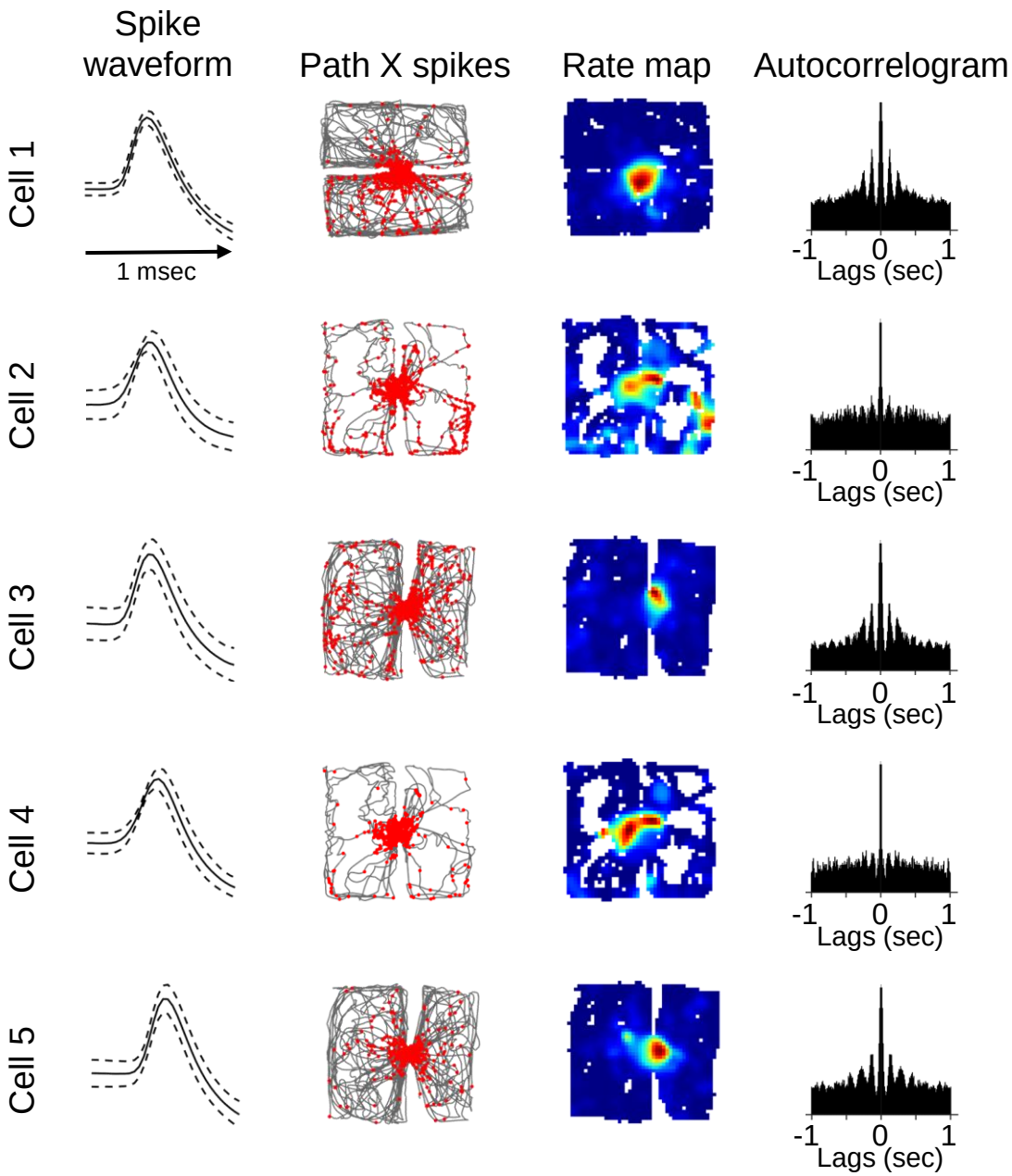


**Supplementary figure 8 – 5 place cells with a place field located at the door in the 2 connected room environment.**

The 5 place cells excluded from analyses because they have a place field located at the door in the 2 connected room environment. For each place cell is shown cell waveform (left column), animal path (grey line) with spike superimposed (red dots) (middle-left), rate maps coded according to a color scale that goes from blue (0Hz) to red (maximum rate), with cyan, yellow and orange as intermediate firing from low to high (middle-right), and autocorrelograms of the firing activity in 1-s lags (right).

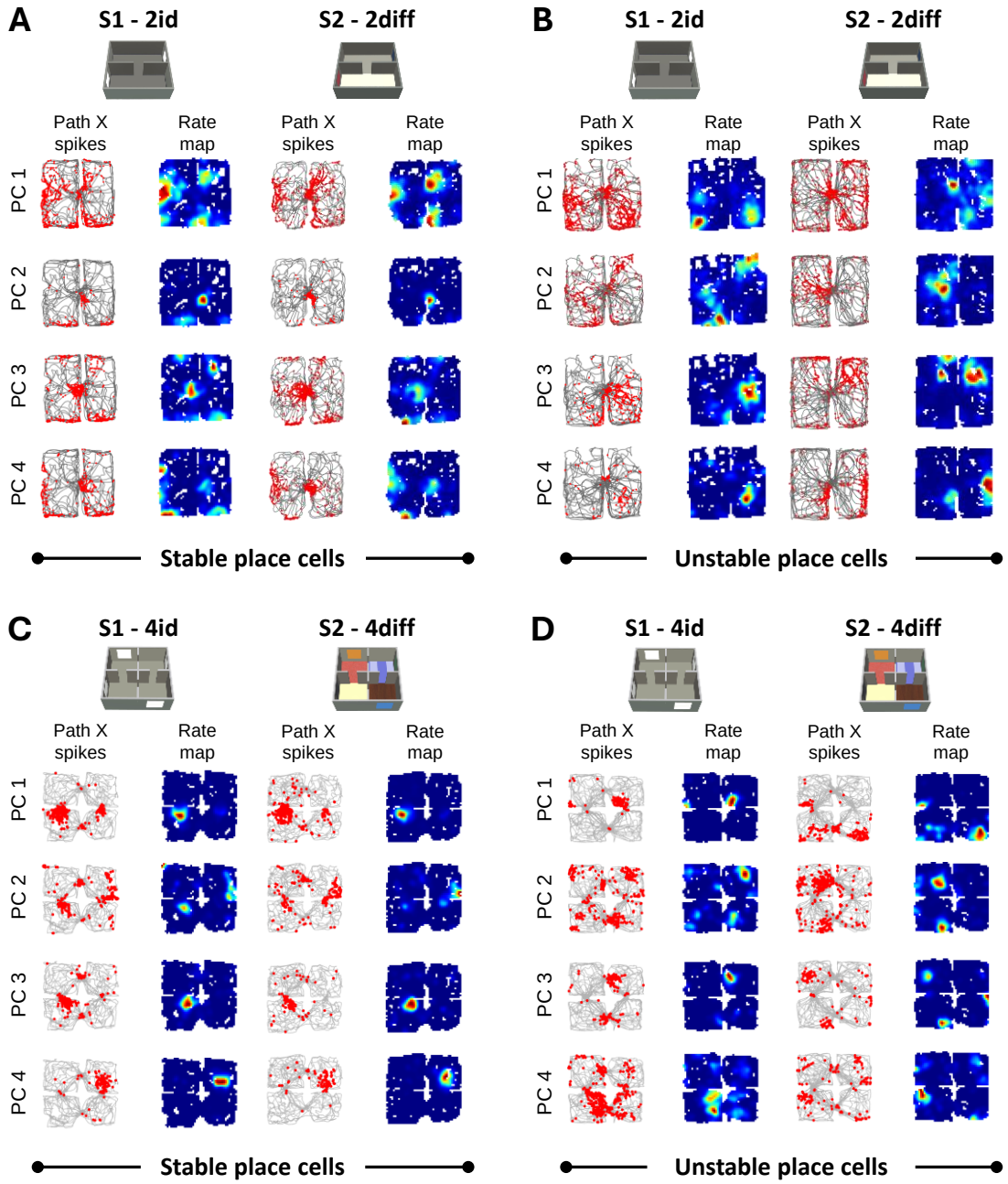


**Supplementary figure 9 – Place cells (PC) stability between identical and different connected rooms environment is session dependent.**
Examples of the activity of simultaneously recorded PC between identical (left) and different (right) connected rooms environment. Within a given session PCs show either stable place field(s) (**A-C**) and unstable place field(s) (**B-D**). For each place cell is shown animal path (grey line) with spike superimposed (red dots) (left) and rate maps coded according to a color scale that goes from blue (0Hz) to red (maximum rate).